Self-organization and Fourier selection of optical patterns in a nonlinear photorefractive feedback system

O. Sandfuchs and F. Kaiser
Institute of Applied Physics, Darmstadt University of Technology, Hochschulstrasse 4a, 64289 Darmstadt, Germany

M. R. Belić
Institute of Physics, P.O. Box 57, 11001 Belgrade, Yugoslavia
(Received 22 June 2001; published 15 November 2001)

The formation of patterns in two transverse dimensions in photorefractive two-wave mixing with a single feedback mirror is investigated theoretically. We perform numerical simulations of the full (3+1)-dimensional nonlinear model equations, displaying the breakup of the unstable annulus of active modes into hexagonal spots. Analytically we derive amplitude equations of the Landau type for patterns with rhombic- and hexagonal-mode interaction and discuss the stability and coexistence of transverse planforms in the photorefractive feedback system. A strong renormalization for the hexagon amplitude is determined, and its consequences for pattern formation using Landau formalism are discussed. In particular, the stability of regular substructures of a dodecagonal spot arrangement is investigated and square-hexagon competition is predicted. We use an invasive Fourier-filtering technique for the selection of unstable patterns, such as stripes and squares. The longitudinal propagation of the critical and higher-order modes of the self-organized structures and the impact of a Fourier filter on the mode propagation within a nonlinear bulk photorefractive medium is studied in detail.

DOI: 10.1103/PhysRevA.64.063809 PACS number(s): 42.65.Sf, 42.70.Nq, 42.40.Pa

I. INTRODUCTION

Spontaneous pattern formation is the topic of intensive research in many fields of science concerned with dissipative structures in nonequilibrium systems. Much effort has been addressed to a universal understanding of the formation of complex spatiotemporal patterns [1–3]. In the vicinity of a bifurcation point, the concept of order-parameter equations of synergetics [4] has been widely applied and proven a useful tool in analyzing the mode-selection mechanisms and the stability of patterns in various physical systems, such as surface waves [5], ferromagnetic systems [6,7], reaction-diffusion systems [8,9], Bénard-Marangoni convection [10], and nonlinear optical systems [11–14]. Despite its universal character, the question of pattern selection and competition for a specific system still remains one of the interesting and demanding problems.

Symmetries and the type of bifurcation determine the form of the order-parameter equations. The coefficients reflect the specific characteristics of the underlying system and play an important role for the pattern-selection process. Periodic planar patterns, such as stripes, rhombi, squares, and hexagons possess a translational symmetry. Among these regular structures the hexagonal patterns have played an outstanding role, not merely because of the beauty of their arrangement but also because of their specific properties, such as the broken inversion symmetry and the resonant interaction between fundamental modes, which makes them the dominant patterns in systems that physically support the breaking of inversion symmetry.

The natural coexistence of stripes and hexagons has widely been discussed in terms of Landau hexagon equations, see, e.g., Ref. [15]. The possible coexistence of squares and hexagons is more involved and has attracted considerable attention recently. Theoretical studies of the competition of these two types of patterns, which belong to different symmetry classes [16] and cannot simultaneously exist on a spatially periodic lattice, may lead to spatially aperiodic patterns (quasipatterns) of 12-fold symmetry, such as dodecagons [17–19]. Their existence has been confirmed in a variety of experimental observations in different pattern-forming systems within recent years [20–22].

Ever since the initial experimental observations of hexagonal patterns [23–25] due to counterpropagation of two optical beams in photorefractive (PR) crystals, pattern formation through PR two-wave mixing has become a growing field of nonlinear optics [26–28]. In particular, the formation of patterns in a PR crystal with an external feedback mirror has been the topic of a number of recent articles. Structures such as stripes and squares have been identified [26,29], and very recently experiments on the competition of dynamical patterns [29,30], multistability [31], and the appearance of dodecagons have been reported [32]. PR crystals hold promise for parallel optical data and image processing, hence the interest in transverse spatiotemporal structures in such media.

Experiments have been accompanied by theoretical analyses of transverse modulational instabilities [33–35]. However, there are only a few theoretical investigations beyond linear instability that analyze and explain the appearance of the variety of patterns. In a paper by Lushnikov [36] the stabilization of the hexagonal-mode structure is explained using an amplitude-equation formalism. Three coupled Landau equations were derived describing the coexistence of stripes and hexagons. It was stated that the corresponding coefficients are valid more qualitatively than quantitatively due to a substantial renormalization. Saturation of explosive instabilities, for which higher-order wave processes are nec-

essary, was obtained by a numerical experiment taking into account a larger number of sum and difference harmonics in the series expansion.

The cooperative effect of diffraction and nonlinear beam coupling leads to the formation of transverse patterns. Owing to diffraction of optical beams, patterns arise in a plane perpendicular to the propagation direction. The optical beams become spontaneously unstable against transverse modulations that grow due to an absolute instability out of the initially smooth beam and grating profiles. The two-wave mixing between forward and backward propagating optical beams induces a refractive-index grating, which in turn couples the beams by Bragg diffraction [37]. Bragg diffraction is present because of the finite longitudinal extent of the crystal, i.e., a volume-index grating is formed whose grating period is much shorter than the medium length. The counterpropagation of optical beams and the choice of crystal orientation favors the formation of reflection gratings. The coupling between beams leads to an exchange of energy and the pump beam is depleted. This pump depletion is not negligible when dealing with pattern formation in a PR system with optical feedback. It is the origin of tremendous difficulties in the theoretical treatment, both analytical and numerical.

Another important feature of PR wave mixing that is usually neglected, because of the difficulties in analytical and numerical treatment, regards the temporal evolution of the refractive-index grating, which is dependent on the total light intensity. The nonuniform distribution of the total light intensity, due to pump depletion along the propagation direction and spatiotemporal modulation in the transverse plane, results in a photorefractive time constant that varies whithin the crystal. The PR medium reacts faster in more illuminated regions and the buildup of refractive-index changes proceeds at different paces. The transient dynamics of one-dimensional spatiotemporal patterns has been shown to slow down by a few orders of magnitude compared to the model with constant relaxation time [38], however the coexistence of stationary patterns and the Fourier selection is not affected. Therefore, we will present numerical simulations for the model with the constant-relaxation-time approximation.

In recent years research activities have focused on the manipulation and control of patterns in spatially extended continuous systems [39–44]. Triggered by methods of chaos control [45,46], which have been successfully applied to stabilize unstable orbits in purely temporal dynamics, it is desirable to establish analogous methods for stabilization of unstable states in spatiotemporal systems. The amplitude-equation formalism, where applicable, provides an analytical method to obtain the unstable pattern states, so that the patterns can be directly compared when selection and stabilization methods are applied. Such methods would exert an impact on technological applications in, for example, information processing, for which optical devices have promising perspectives.

Although manipulation of spatial structures in the Fourier domain is now one of the most important concepts in modern nonlinear optics, a rigorous theoretical proof of its power to stabilize unstable eigensolutions is still missing. This is particularly true for wave mixing with a PR nonlinearity, where the patterning process takes place in a medium of finite longitudinal extent. Here the Fourier filter acts as a strong or weak disturbance of the mirror boundary conditions in the case of invasive or noninvasive control methods, respectively. We will not give this proof here but instead discuss some advantages and problems that the Fourier-filtering technique, which has been used so far in experiments with the PR feedback system [40,47–49], poses from a theoretical point of view.

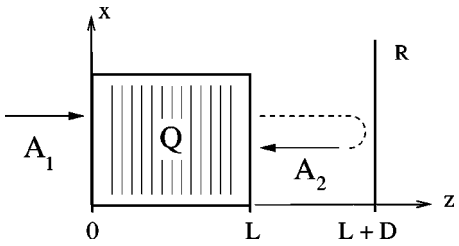

FIG. 1. Two-wave mixing configuration in the reflection geometry with a feedback mirror M. A_1 is the pump and A_2 is the reflected beam, Q is the grating amplitude, z indicates the direction of propagation, and x is one of the two transverse dimensions. L is the crystal length and D is the distance to the feedback mirror.

Our investigation proceeds along two tracks, analytical and numerical. After introducing the model of the PR feedback system (Sec. II), we perform a linear stability and a nonlinear amplitude analysis, and discuss the threshold behavior and the stability of N-modal transverse patterns by means of a Landau description, thereby neglecting slow spatial variations (Secs. III and IV). Numerically, we discuss the self-organization of PR hexagons (Sec. V) and the effects of Fourier filtering on regular patterns in a bulk PR medium (Sec. VI). Section VII brings conclusions.

II. WAVE-MIXING EQUATIONS

The model for the PR wave mixing through the formation of a reflection grating originates from the charge-transport model of Kukhtarev *et al.* [50]. Rigorous solution of Kukhtarev's nonlinear material equations is computationally expensive [51], particularly in the context of transverse-pattern formation in the PR feedback system. Hence the need for an approximation of the grating response, which is as simple as possible, but good enough to account for the interesting phenomena observed in pattern formation. Such a model of wave mixing is introduced below.

The setup for observation of transverse patterns in PR two-wave mixing (2WM) with a single feedback mirror is presented in Fig. 1. The wave-mixing process is described by the slowly varying envelope paraxial equations for the two beams [38] in two transverse dimensions

$$\partial_z A_1 + i f \nabla_\perp^2 A_1 = -Q A_2, \tag{1a}$$

$$-\partial_z A_2 + i f \nabla_\perp^2 A_2 = Q^* A_1, \tag{1b}$$

where z is the propagation coordinate scaled by the crystal length L, and $\nabla_\perp^2$ is the transverse Laplacian scaled by the

beam waist w_0. The parameter $f=L/(2k_0w_0^2)$ represents a measure of the magnitude of diffraction and is proportional to the inverse of the Fresnel number. Here k_0 denotes the wave number in the longitudinal direction within the crystal. Absorption losses have been neglected. Q is the complex amplitude of the reflection grating, whose temporal evolution is described by a relaxation equation of the form

$$\tau(I)\partial_t Q+Q=\Gamma\frac{A_1A_2^*}{|A_1|^2+|A_2|^2+I_d}, \tag{2}$$

where Γ is the wave coupling constant. In PR wave mixing, charge-transport processes yield an, in general, intensity-dependent relaxation time $\tau(I)=(I_p/I)^\kappa\tau_{PR}$, with the total intensity $I=|A_1|^2+|A_2|^2+I_d$. The exponent κ describes the characteristic behavior of nonlinear charge-diffusion processes present in PR materials. In the standard Kukhtarev model, assuming linear medium response, the time constant is calculated to be inversely proportional ($\kappa=1$) to the total intensity. Nonlinear material response and nonlinear charge-diffusion processes lead to values of $\kappa\neq1$. In particular, numerical investigation of Kukhtarev's band-transport model yielded a sublinear dependence [51] with $\kappa\approx0.7$, which is characteristic of slowed diffusion processes.

The dark intensity I_d, due to thermal background illumination, is considered small ($I_d\sim10^{-5}I_p$) as compared to the intensity of the input pump beam, $I_p=|A_1(x,y,z=0)|^2$. Since τ_{PR} is a constant that depends only on material properties, it defines a natural scaling of time.

The assumption in Eqs. (1) and (2) is that the dynamics of envelopes is slaved to the grating amplitude because of its slow evolution, and that the spatial distribution of Q is determined by the spatial distribution of the beam envelopes, with the Debye-screening length much shorter than the wavelength of a transverse pattern. Although this model may look extremely simple, it still requires much computational effort. Since the first experimental evidence of hexagonal patterns in 1993 [23], to our knowledge we believe ourselves to be the first ones to present numerical simulations of transverse patterns in 3+1 dimensions.

III. LINEAR STABILITY ANALYSIS

Linear stability of two counterpropagating optical beams with a PR nonlinearity has been discussed in a variety of previous works [33–35]. Analytical threshold conditions were obtained under certain constraints. Mirror reflectivities lower than unity and the effect of intensity dependence of the PR relaxation time immediately result in a nonautonomous stability problem, and analytical expressions no longer exist. In the following we present a semianalytical approach to find the primary threshold for the onset of two-dimensional transverse patterns in the feedback system without imposing such constraints. Thus we are able to discuss important effects concerning different mirror reflectivities and intensity-dependent PR relaxation time.

The primary threshold is determined by the linear instability of the steady-state plane-wave field amplitudes, denoted by $A_1^0(z)$ and $A_2^0(z)$, and the corresponding amplitude of the refractive-index grating $Q^0(z)$. The linear eigenspace constitutes the base for the subsequent nonlinear bifurcation analysis. Therefore we consider the time and space evolution of the perturbations $a_{1,2}$ and q from the homogeneous fixed-point amplitudes,

$$A_{1;2}(x,y,z,t)=A_{1;2}^0(z)[1+a_{1;2}(x,y,z,t)], \tag{3a}$$

$$Q(x,y,z,t)=Q^0(z)[1+q(x,y,z,t)]. \tag{3b}$$

After substituting Eqs. (3) into Eqs. (1) and (2) the perturbations are expanded in the transverse Fourier and in the temporal Laplace space ($t\rightarrow\lambda$), where q can be eliminated, and the linearized propagation of perturbations is cast into a matrix form

$$\partial_z\mathbf{a}=\mathcal{A}(z,K^2,\lambda)\mathbf{a}(z,K^2,\lambda), \tag{4}$$

where K^2 is the square of the transverse wave vector. The vector $\mathbf{a}=(a_1,a_1^*,a_2,a_2^*)^T$ then contains the Fourier-Laplace components of the perturbations. Choosing an appropriate basis via a transformation $\mathcal{U}$ (see Appendix A), the physics involved in the linear stability analysis for PR wave mixing becomes more obvious. The stability matrix reads as

$$\mathcal{A}=\mathcal{U}^{-1}\begin{pmatrix} m_0^2\Gamma+(1-m_0^2)g(\lambda) & -fK^2 & 0 & 0 \\ fK^2 & 0 & 0 & -\sqrt{1-m_0^2}g(\lambda) \\ -\sqrt{1-m_0^2}g(\lambda) & 0 & 0 & -fK^2 \\ 0 & 0 & fK^2 & g(\lambda) \end{pmatrix}\mathcal{U}. \tag{5}$$

Note that the steady-state fixed-point solution contributes to stability through its modulation depth

$$m_0(z)=\frac{2\sqrt{I_1^0(z)I_2^0(z)}}{I_1^0(z)+I_2^0(z)} \tag{6}$$

and through the temporal variations in Q that are, due to the PR medium response, given by

$$g(\lambda)=\Gamma\frac{\lambda\tau(I^0)}{\lambda\tau(I^0)+1}. \tag{7}$$

Owing to pump depletion, the fact that $m_0(z)\leqslant1$, and the

intensity-dependent relaxation time, the nonautonomous Eq. (4) cannot in general be solved analytically. Nonetheless, a formal solution is given by $\mathbf{a}(L)=\mathcal{F}(L)\mathbf{a}(0)$, where $\mathcal{F}(z)$ is the linear flow matrix. Hence the problem of linear stability is solved if $\mathcal{F}(L)$ is known. Separating $\mathcal{A}$ into $\mathrm{tr}\,\mathcal{A}$ and its trace-free part $\mathcal{A}_f=\mathcal{A}-\mathrm{tr}\,\mathcal{A}/4$, the linear flow matrix can be calculated from

$$\mathcal{F}(L)=\exp\left(\int_0^L \mathrm{tr}\,\mathcal{A}(s)ds\right)\times\prod_{z=0}^{L}\delta\mathcal{G}(z). \tag{8}$$

Since both $m_0(z)$ and $\tau[I^0(z)]$ are monotonous functions, one is not faced with the Floquet problem, and the product can be obtained through a repeated multiplication of infinitesimal rotation matrices $\delta\mathcal{G}(z)=\exp[\int_z^{z+\delta z}\mathcal{A}_f(s)ds]$, taken at subsequent points z in the crystal. These matrix products have to be evaluated numerically. Taking into account the mirror boundary conditions

$$a_1(x,y,0,t)\equiv 0, \tag{9a}$$

$$a_2(x,y,L,t)=(T_F)^{-1}\{\exp(i\phi)T_F[a_1(x,y,L,t)]\}, \tag{9b}$$

one inverts $\mathcal{F}(L)$ into a scattering matrix $\mathcal{S}$. The quantity $\phi=2fK^2D/(n_0L)$ is the propagation phase, D being the distance from the crystal to the feedback mirror, T_F denotes the Fourier transform, and n_0 is the crystal's homogeneous refractive index. The poles of the scattering matrix determine the properties of an absolute instability and lead to the threshold condition (in the $\mathcal{U}$ basis),

$$\det[\mathcal{F}_{11}+\mathcal{F}_{22}-\mathcal{F}_{12}-\mathcal{F}_{21}-\mathcal{D}(\phi)(\mathcal{F}_{11}-\mathcal{F}_{22}-\mathcal{F}_{12}+\mathcal{F}_{21})]=0, \tag{10}$$

where $\mathcal{F}_{jk}$ are 2×2 submatrices of $\mathcal{F}(L)$ and

$$\mathcal{D}(\phi)=\begin{pmatrix}-\cos(\phi) & \sin(\phi)\\ \sin(\phi) & \cos(\phi)\end{pmatrix} \tag{11}$$

is a matrix involving the propagation phase. Under special constraints for the mirror reflectivity $R=1$, which implies that the modulation depth $m_0(z)\equiv 1$, and for the constant-relaxation-time approximation ($\kappa=0$), Eq. (10) can be expressed analytically [38].

The threshold behavior at the primary instability is displayed in Fig. 2 for the case $D=0$. It does not depend on the characteristic exponent κ for the PR relaxation time, because for any R one finds only stationary bifurcations. For $R=1$ the homogeneous plane-wave solution loses stability at the threshold coupling constant $\Gamma_c L\approx 3.819$. A small band around the critical transverse wave vector $fK_c^2\approx 2.592$ becomes unstable [Fig. 2(a)]. In two transverse dimensions this corresponds to an annulus of unstable modes, from which the nonlinear-mode interaction creates a specific pattern.

In experiments, because of Fresnel reflections and beam-intensity losses from optical components in the feedback loop [29], the effective mirror reflectivity is typically lower than unity. The threshold, however, turns out to be only weakly changed by the reduction of mirror reflectivity all the way down to about $R=0.1$, and it noticeably increases only for much lower reflectivities [Fig. 2(b)]. The reason for this lies in the PR gain of two counterpropagating beams, so that only for small values of R the modulation depth in the interaction region starts deviating from unity. The spatial frequency of transverse modulations remains nearly unaffected.

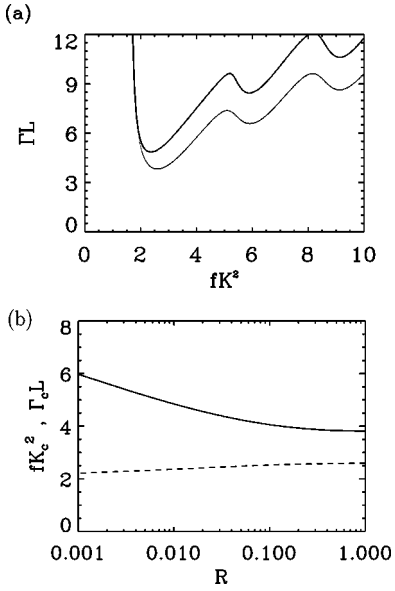

FIG. 2. Threshold curve for $D=0$. (a) Coupling strength Γ as a function of the transverse wave number K for a stationary instability with $R=1$ (lower curve) and $R=0.01$ (upper curve). (b) Dependence of the critical values Γ_c (solid) and K_c (dashed) on the mirror reflectivity R.

When the mirror is moved towards larger feedback distances ($D>0$), the type of threshold that is predicted by linear stability analysis strongly depends on the model for the temporal evolution. In the case of the model with $\kappa=0$ there exists a critical mirror distance $D_c\approx 0.25$ at which an oscillatory instability should occur (Fig. 3) and the threshold values differ considerably. This, however, is an artifact of the constant-relaxation-time approximation, and it is prominent for reflectivities above 90%. The model that takes into account the inverse intensity dependence ($\kappa=1$) displays only stationary structures. This is in perfect agreement with experimental observations [25,26,31]. For reflectivities below 90%, any value of κ will give the same stationary instability threshold. In Fig. 3 we have shown the case for $R=0.5$. The critical coupling strength slightly deviates for large mirror distances, but the spatial frequency, i.e., the angle between pump and sideband beams in the optical far field, is almost indistinguishable. So, discrepancies in the sideband angle arising between theory and experiment presumably do not originate from a nonideal feedback mirror.

IV. AMPLITUDE EQUATIONS

The question what patterns, be they stable or unstable, will be formed out of the annulus of active modes can be answered by a nonlinear bifurcation analysis. In the following we present a detailed derivation of coupled Landau equa-

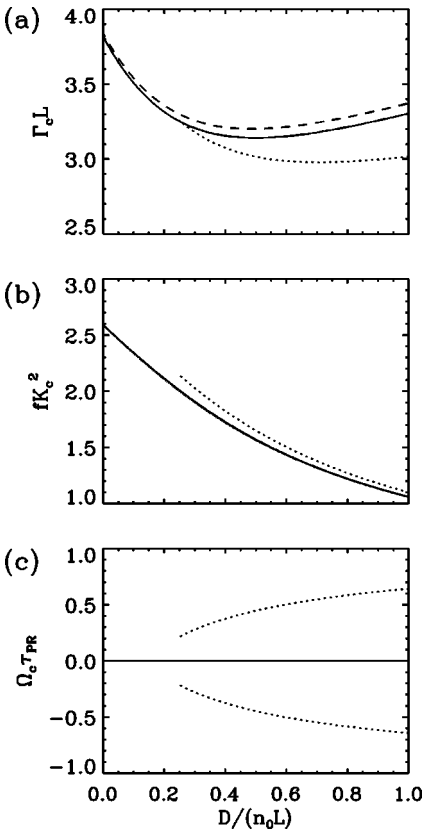

FIG. 3. Threshold curves as functions of the mirror distance D for the models assuming different intensity dependence of the relaxation time: the model with $\kappa=0$ (dotted line) for $R=1.0$, the model with $\kappa=1$ (solid line) for $R=1.0$. The dashed line is for $R=0.5$ with any of the two κ models. (a) Critical coupling strength Γ_c, (b) critical wave number K_c, and (c) oscillation frequency Ω_c.

tions for different two-dimensional planforms. Proper normalization and renormalization of the longitudinal eigenfunctions will play an important role in determining the coefficients for Landau equations, so that they can be quantitatively compared with numerical simulations of the full nonlinear-model equations.

The nonlinear bifurcation analysis considers the time and space evolution of deviations from the fixed-point plane-wave solutions. Upon substituting Eqs. (3) into Eqs. (1) and (2), and retaining all nonlinear terms, one obtains

$$\partial_z a_1 + if\nabla_\perp^2 a_1 = \frac{\Gamma}{1+r^0}(a_1 - a_2 - q - a_2 q), \tag{12a}$$

$$-\partial_z a_2 + if\nabla_\perp^2 a_2 = \frac{\Gamma r^0}{1+r^0}(a_1 - a_2 + q^* + a_1 q^*), \tag{12b}$$

$$\left(\frac{1+r^0}{N_A}\right)^\kappa \tau(I^0)\partial_t q + q = \frac{(a_1-a_2)(1+a_2^*) - r^0(a_1^*-a_2^*)(1+a_1)}{r^0(1+a_1)(1+a_1^*) + (1+a_2)(1+a_2^*)}, \tag{12c}$$

where $I^0(z)=|A_1^0(z)|^2+|A_2^0(z)|^2$ is the total plane-wave intensity, and $r^0(z)=|A_1^0(z)|^2/|A_2^0(z)|^2$ is the ratio of plane-wave intensities. The denominator N_A is identical to the denominator of the right-hand side (rhs) of Eq. (12c). For the general procedure of multiple-scale analysis in a bulk medium, where we follow an idea of Geddes *et al.* [11], which is modified to account for the PR wave-mixing and grating dynamics, it is convenient to choose a real basis for the state vectors of deviations via the following transformation (see Appendix A): $(a_1, a_1^*, a_2, a_2^*)^T \to \vec{U}=(U_1,U_2,U_3,U_4)^T$ and $(q,q^*)^T \to \vec{P}=(P_1,P_2)^T$, which brings Eqs. (12) into the general form,

$$\mathcal{L}_{z;x,y}\vec{U} + \mathcal{M}_0\vec{P} = \vec{\mathcal{M}}_1(\vec{P}|\vec{U}), \tag{13a}$$

$$[\mathcal{D}_{0,t} + \mathcal{D}_{1,t}(\vec{U}) + \mathcal{D}_{2,t}(\vec{U}|\vec{U}) + \cdots]\vec{P} - \mathcal{N}_0\vec{U} = \vec{\mathcal{N}}_1(\vec{U}|\vec{U}) + \vec{\mathcal{N}}_2(\vec{U}|\vec{U}|\vec{U}) + \cdots. \tag{13b}$$

Here the matrices $\mathcal{L}_{z;x,y}$ and $\mathcal{D}_{j,t}$ are the spatial- and temporal-derivative operators, respectively. Owing to the intensity dependence of the PR relaxation time, the temporal evolution contributes to linear $\mathcal{D}_{0,t}$ and nonlinear $\mathcal{D}_{j,t}$ terms ($j=1,2,\ldots$). The matrices $\mathcal{M}_0$ and $\mathcal{N}_0$ are composed of the coefficients of the linear coupling between the field and the grating, and $\vec{\mathcal{M}}_1$ and $\vec{\mathcal{N}}_j$ are the vectors describing nonlinear field-grating and field-field interactions. The notations $(\vec{U}|\vec{U})$ and $(\vec{U}|\vec{U}|\vec{U})$ are shorthands for different quadratic and cubic terms arising in such a procedure.

The multiple-scale analysis is based on the fact that in the neighborhood of a bifurcation point, the spatiotemporal evolution is separable into fast and slow scales. The PR coupling strength Γ is the bifurcation parameter, and the expansion parameter ϵ scales the distance from the critical point Γ_c at which the modulational instability starts growing. Considering a spatially homogeneous distribution of modulation, in order to describe the pattern through a Landau-type formalism, one expands the bifurcation parameter, the temporal variable, and the field and grating amplitudes in powers of ϵ,

$$\Gamma = \Gamma_c + \epsilon\Gamma^{(1)} + \epsilon^2\Gamma^{(2)} + \cdots, \tag{14a}$$

$$t = T_0 + \epsilon T_1 + \epsilon^2 T_2 + \cdots, \tag{14b}$$

$$\vec{U} = \epsilon^\nu \vec{U}^{(1)} + \epsilon^{2\nu}\vec{U}^{(2)} + \epsilon^{3\nu}\vec{U}^{(3)} + \cdots, \tag{14c}$$

$$\vec{P} = \epsilon^\nu \vec{P}^{(1)} + \epsilon^{2\nu}\vec{P}^{(2)} + \epsilon^{3\nu}\vec{P}^{(3)} + \cdots. \tag{14d}$$

The $\Gamma^{(j)}$ are as yet unknown quantities to be determined by the multiple-scale analysis. In the case of stripe patterns, e.g., one usually chooses the scaling exponent such that $\nu=1/2$, therefore, *a priori* assuming the specific scaling behavior of a pitchfork bifurcation. We have taken $\nu=1$, which leads to the same amplitude equation and, in addition, provides for the correct scaling behavior, corresponding to the characteristics of the underlying bifurcation for both rhombic and hexagonal planforms. The latter bifurcate transcritically, so $\nu=1$ is mandatory (cf. Sec. IV B).

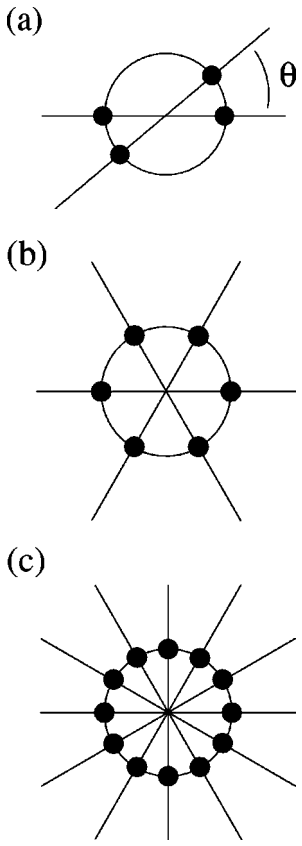

FIG. 4. Arrays of spot pairs on the annulus of active modes: (a) Rhombic planform ($N=2$) with the angle θ between the spot pairs. (b) Hexagonal ($N=3$) and (c) Dodecagonal ($N=6$) mode distributions.

Even though the terms are grouped in Eq. (13b) according to their nonlinear order, these equations still describe the evolution of all combinations of modes, and hence of all possible patterns. To study a particular pattern, one introduces order parameters $W_j=W_j(T_1,T_2,\ldots)$, which are proportional to the amplitudes of critical modes on the annulus, and may still depend on the slower time scales. Stationary equilateral patterns require that the amplitude W_j belonging to K_c and the amplitude W_j^* belonging to $-K_c$ have the same magnitude. So, the mode amplitudes occur in pairs.

In the first order of ϵ one recovers the linear problem

$$\mathcal{L}^c_{z;x,y}\vec{U}^{(1)}+\mathcal{M}^c_0\vec{P}^{(1)}=0, \tag{15a}$$

$$\mathcal{D}_{0,T_0}\vec{P}^{(1)}-\mathcal{N}_0\vec{U}^{(1)}=0. \tag{15b}$$

Eliminating $\vec{P}^{(1)}$ with $T_0\to\lambda$ recovers the linear instability problem, Eq. (4),

$$[\mathcal{L}_z(K^2)+\mathcal{M}_0\mathcal{D}_0(\lambda)^{-1}\mathcal{N}_0]\vec{U}^{(1)} \equiv[\partial_z-\mathcal{A}(z;K^2,\lambda)]\vec{U}^{(1)}=0. \tag{16}$$

Higher orders in ϵ describe the nonlinear interaction of spatial modes and result in the amplitude equation for each of the order parameters. In the second order it is

$$\mathcal{L}^c_{z;x,y}\vec{U}^{(2)}+\mathcal{M}^c_0\vec{P}^{(2)}=\mathcal{L}^{(1)}\vec{U}^{(1)}-\mathcal{M}^{(1)}_0\vec{P}^{(1)} +\vec{\mathcal{M}}_1(\vec{P}^{(1)}|\vec{U}^{(1)}), \tag{17a}$$

$$\mathcal{D}_{0,T_0}\vec{P}^{(2)}-\mathcal{N}_0\vec{U}^{(2)}=-\mathcal{D}_{0,T_1}\vec{P}^{(1)}-\mathcal{D}_{1,T_0}(\vec{U}^{(1)})\vec{P}^{(1)} +\vec{\mathcal{N}}_1(\vec{U}^{(1)}|\vec{U}^{(1)}). \tag{17b}$$

For a stationary pattern one has $\mathcal{D}_{0,T_0}=1$, and in Eq. (17b) one can solve for the grating variable $\vec{P}^{(2)}$ and eliminate it from Eq. (17a), in favor of an inhomogeneous ordinary differential equation for the field variable $\vec{U}^{(2)}$. Stable saturation of the linear exponential growth for any regular-shaped pattern is at first achieved in the third order. From the expansion one finds

$$\mathcal{L}^c_{z;x,y}\vec{U}^{(3)}+\mathcal{M}^c_0\vec{P}^{(3)}=\mathcal{L}^{(2)}\vec{U}^{(1)}-\mathcal{M}^{(2)}_0\vec{P}^{(1)} +\vec{\mathcal{M}}^c_1(\vec{P}^{(1)}|\vec{U}^{(2)})+\vec{\mathcal{M}}^c_1(\vec{P}^{(2)}|\vec{U}^{(1)}), \tag{18a}$$

$$\begin{aligned}\mathcal{D}_{0,T_0}\vec{P}^{(3)}-\mathcal{N}_0\vec{U}^{(3)}=&-\mathcal{D}_{0,T_2}\vec{P}^{(1)}-\mathcal{D}_{0,T_1}\vec{P}^{(2)}\\ &-\mathcal{D}_{1,T_0}(\vec{U}^{(1)})\vec{P}^{(2)}-\mathcal{D}_{1,T_0}(\vec{U}^{(2)})\vec{P}^{(1)}\\ &-\mathcal{D}_{1,T_1}(\vec{U}^{(1)})\vec{P}^{(1)}\\ &-\mathcal{D}_{2,T_0}(\vec{U}^{(1)}|\vec{U}^{(1)})\vec{P}^{(1)}\\ &+\vec{\mathcal{N}}_1(\vec{U}^{(1)}|\vec{U}^{(2)})+\vec{\mathcal{N}}_1(\vec{U}^{(2)}|\vec{U}^{(1)})\\ &+\vec{\mathcal{N}}_2(\vec{U}^{(1)}|\vec{U}^{(1)}|\vec{U}^{(1)}).\end{aligned} \tag{18b}$$

A specific stationary pattern may consist of any combination of N spot pairs on the annulus. To determine which of them will result in a stable configuration, one derives the cubic self- and cross-coupling coefficients of all possible mode interactions. Herefore it is sufficient to calculate the coefficients for the bimodal interaction ($N=2$) and, in the case when a resonant interaction occurs for the hexagonal structure, the coefficients for the trimodal interaction ($N=3$).

A. Stripes, squares, and rhombic planforms

We start out by calculating the coefficients for the interaction of bimodal structures [Fig. 4(a)] that consist of two pairs of critical wave vectors, and thus make the specific ansatz for the stationary rhombic pattern,

$$\vec{U}^{(1)}=\vec{u}^{(1)}(z;K_c)\left(\sum_{j=1}^{2}W_j\exp(iK_c\rho_j)+\text{c.c.}\right), \tag{19}$$

$$\vec{P}^{(1)}=\vec{p}^{(1)}(z;K_c)\left(\sum_{j=1}^{2}W_j\exp(iK_c\rho_j)+\text{c.c.}\right). \tag{20}$$

The direction of the two mode pairs has been chosen so that $\rho_1=x$ and $\rho_2=x\cos\theta+y\sin\theta$, where θ is the angle between

the pairs. Square patterns are obtained for $\theta=\pi/2$ and stripes represent a degenerate case when the two spot pairs merge ($\theta=0$ or π).

The development of a transverse modulation in the light fields during the propagation through the bulk PR medium in this order is described by the longitudinal eigenfunction $\vec{u}^{(1)}(z;K_c)$ of the critical mode. The propagation of modulations in the refractive index is captured by $\vec{p}^{(1)}(z;K_c)=\mathcal{N}_0\vec{u}^{(1)}(z;K_c)$. The eigenfunction $\vec{u}^{(1)}$ can be obtained from the flow matrix of the linear stability problem,

$$\vec{u}^{(1)}(z,K_c)=\mathcal{F}(z;K_c)\vec{u}^{(1)}(0), \tag{21}$$

where the vector of initial condition $\vec{u}^{(1)}(0)$ belongs to the kernel of the (inverse of the) scattering matrix $\mathcal{S}(K_c)$. Thus the eigenfunction $\vec{u}^{(1)}(z,K_c)$ is defined up to an arbitrary factor μ. In pattern formation there exists no physical condition to determine its value. Realizing that the real parts of the deviations $a_{1,2}$ resemble the intensity modulation of the beam profile $\delta I_j/I_j^0=2\,\mathrm{Re}\,a_j+|a_j|^2$, with $|a_j|^2$ being small near threshold, the normalization of eigenfunctions in the first order, using the condition that $\mathrm{Re}\,a_2(z=0,K_c)=1$, leads to the value $\mu=\mu^{(1)}=0.0558$ (for $D=0$). The Landau coefficients then provide a stationary-mode amplitude, which can be directly compared with numerical simulations or experimental results. It turns out to be a perfect choice for the case of supercritical stripes and rhombi, but, unfortunately, a bad choice for the subcritical hexagons. We will resume this discussion in more detail in Secs. V B and V C.

As soon as one goes to higher orders in the expansion, nonlinear-mode interaction occurs, and spatial Fourier modes $K=0$, K_c, $2K_c$, and $K_\pm=K_c\sqrt{2(1\pm\cos\theta)}$ are generated. Consequently, the solution ansatz in the second order is of the form

$$\begin{aligned}\vec{U}^{(2)}=&\vec{u}^{(2)}(z;K=0)(|W_1|^2+|W_2|^2+\text{c.c.})+\vec{u}^{(2)}(z;K_c)\\&\times[V_1\exp(iK_c\rho_1)+V_2\exp(iK_c\rho_2)+\text{c.c.}]\\&+\vec{u}^{(2)}(z;2K_c)[W_1^2\exp(2iK_c\rho_1)\\&+W_2^2\exp(2iK_c\rho_2)+\text{c.c.}]+\vec{u}^{(2)}(z;K_+)\\&\times\{2W_1W_2\exp(iK_c[\rho_1+\rho_2])+\text{c.c.}\}+\vec{u}^{(2)}(z;K_-)\\&\times\{2W_1W_2^*\exp(iK_c[\rho_1-\rho_2])+\text{c.c.}\}.\end{aligned} \tag{22}$$

Since the resonant mode is formally generated, the new amplitudes V_j must be introduced. The longitudinal eigenfunctions in the second order then satisfy the equation

$$\partial_z\vec{u}^{(2)}(z;K)=\mathcal{A}_c(z;K)\vec{u}^{(2)}(0;K)+\vec{s}^{(2)}(z;K). \tag{23}$$

The associated boundary-value problem has a solution whenever $K\neq K_c$. For the resonant mode $K=K_c$, one has to apply the solvability condition known as the Fredholm alternative theorem. It reads

$$\langle\vec{v}(z;K_c)|\vec{s}^{(2)}(z;K_c)\rangle=0, \tag{24}$$

which involves the scalar product with the adjoint homogeneous solution $\vec{v}(z;K_c)$ and yields $\Gamma^{(1)}W_j=\partial_{T_1}W_j$. In addition to the Fredholm alternative, to avoid secular terms, it must be required that $\partial_{T_1}W_j=0$, which then puts the unknown $\Gamma^{(1)}=0$, and one can choose $V_j=0$. In this manner the longitudinal eigenfunctions in the second order are completely determined. Their shape and their meaning for the pattern formation will be discussed in Secs. V B and VI.

The saturation of the linear exponential growth is at first achieved in the third order. Here the nonlinear-mode interaction again generates resonant and nonresonant modes. The solvability condition, applied to the resonant mode, determines $\Gamma^{(2)}$ and leads to the coupled amplitude equations for a rhombic pattern,

$$\tau_0\partial_tW_1=(\Gamma-\Gamma_c)W_1-(g_\pi|W_1|^2+g_\theta|W_2|^2)W_1, \tag{25a}$$

$$\tau_0\partial_tW_2=(\Gamma-\Gamma_c)W_2-(g_\pi|W_2|^2+g_\theta|W_1|^2)W_2. \tag{25b}$$

These are the well-known coupled Landau equations for rhombic planforms. They provide a universal description for the self-organization of bimodal patterns, which is similar to a second-order phase transition [1]. The values of the relaxation rate

$$\tau_0=\frac{1}{g_L}\langle\vec{v}_{K_c}|\mathcal{M}_0^c\tau(I^0)\mathcal{N}_0|\vec{u}_{K_c}^{(1)}\rangle, \tag{26}$$

the nonlinear self-coupling coefficient

$$g_\pi=\frac{1}{g_L}\langle\vec{v}_{K_c}|\vec{m}_\pi-\mathcal{M}_0^c\vec{n}_\pi\rangle, \tag{27}$$

and the nonlinear cross-coupling coefficient

$$g_\theta=\frac{1}{g_L}\langle\vec{v}_{K_c}|\vec{m}_\theta-\mathcal{M}_0^c\vec{n}_\theta\rangle, \tag{28}$$

supplemented with $g_L=\langle\vec{v}_{K_c}|\tilde{\mathcal{M}}_0\mathcal{N}_0-\tilde{\mathcal{L}}|\vec{u}_{K_c}^{(1)}\rangle$, where $\mathcal{L}=\Gamma\tilde{\mathcal{L}}$, for example, reflect the specific properties of the PR 2WM system under consideration (for details on $\vec{m}_\theta$ and $\vec{n}_\theta$ see Appendix A). The order-parameter equations are known to possess three different stationary solutions: the homogeneous state with the amplitude $W_j=0$, the stripes with the amplitudes

$$|W_1|=\sqrt{(\Gamma-\Gamma_c)/g_\pi}\quad\text{and}\quad W_2=0, \tag{29}$$

and the rhombi with the amplitudes

$$|W_1|=|W_2|=\sqrt{(\Gamma-\Gamma_c)/(g_\pi+g_\theta)}, \tag{30}$$

all of them with arbitrary phases.

The cross-coupling coefficient depends only on the angle θ, and reflection and rotational symmetries imply $g(\theta)=g(-\theta)=g(\theta+m\pi)$, with m being an integer. It is plotted in Fig. 5(a) for the parameters $R=1$ and $D=0$, which we

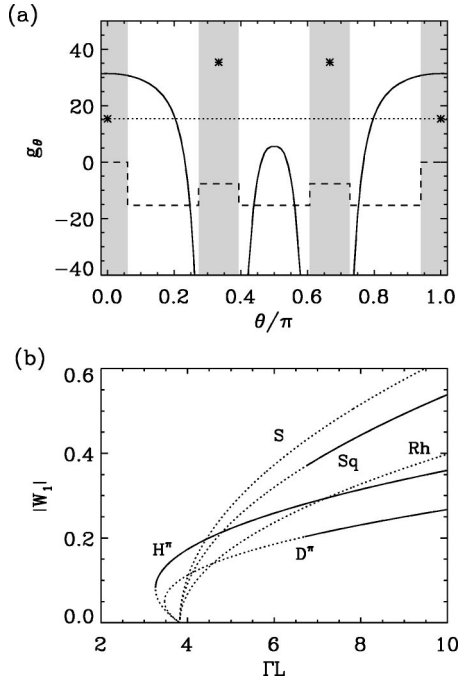

FIG. 5. (a) Cubic cross-coupling coefficient g_θ of Landau-type equations for the bimodal ($N=2$) interaction, with an arbitrary angle θ (solid line) and for $D=0$. The normalization factor for all coefficients is $\mu=\mu^{(1)}\approx 0.0558$. The shaded regions indicate the angular spread of the spots due to the finite mode width. Asterisks (*) denote the coefficients belonging to the unimodal ($N=1$) and trimodal ($N=3$) interactions that dominate in these regions. Above the dashed line the saturation is achieved in the third order. The dotted line indicates the loss of stability of rhombic planforms. (b) Resulting bifurcation diagram for stationary substructures of the dodecagonal spot arrangement ($N=6$, separatrix branches are not shown). H^π, hexagons; D^π, dodecagons; S, stripes; Sq, squares; and Rh, rhombi with an angle $\theta=\pi/6$. Solid (dotted) lines indicate the stable (unstable) branches.

have used in our numerical simulations. Since the number of resonant cubic interactions between two different critical modes is twice the number of self-interactions, $g(\theta)$ is discontinuous at $\theta=0$ and $\theta=\pi$, so that the cross-coupling coefficient $g(\theta\to\pi)=2g_\pi$.

For bimodal structures we find that the cross-coupling coefficient diverges as θ approaches an angle of $\pi/3$, pointing towards the fact that the process of PR wave mixing supports a resonant interaction between the critical modes separated by $\pi/3$. To calculate the coefficient $g_{\pi/3}$ one has to take into account a third active mode, as is presented in the following section. In fact, when the angle θ approaches 0 or $\pi/3$, the modes overlap. Because of the mode degeneracy and the finite beam envelope, the modes have a finite spot size in the K space, and there exists a minimal angular spread $\Delta\theta$ at which the modes start overlapping. So, in the real physical system the function $g(\theta)$ will behave in a continuous way.

B. Hexagonal planform

For pattern formation in the PR feedback system a resonant interaction occurs between the critical modes that form a hexagonal structure. It consists of the superposition of three spot pairs [Fig. 4(b)] rotated by an angle of $2\pi/3$. Therefore, one has to determine the cross-coupling coefficient $g_{\pi/3}$ separately. The ansatz for a stationary hexagonal pattern reads as

$$\vec{U}^{(1)}=\vec{u}^{(1)}(z;K_c)\left(\sum_{j=1}^{3} W_j \exp(iK_c\rho_j)+\text{c.c.}\right), \quad (31)$$

$$\vec{P}^{(1)}=\vec{p}^{(1)}(z;K_c)\left(\sum_{j=1}^{3} W_j \exp(iK_c\rho_j)+\text{c.c.}\right), \quad (32)$$

where the direction of the mode pairs can be chosen as $\rho_1=x$, $\rho_2=(-x+y\sqrt{3})/2$, and $\rho_3=-(x+y\sqrt{3})/2$. The longitudinal eigenfunctions in the first order are again given by Eq. (21).

In the second order, the spatial Fourier modes $K=0, 2K_c$, $K_+=\sqrt{3}K_c$, and $K_-=K_c$ are generated and since the resonant mode is excited, again new amplitudes V_j must be introduced and one has to apply the compatibility conditions in the form of the Fredholm alternative [Eq. (24)]. In contrast to the case of rhombi, for the hexagonal-mode interaction one obtains a nontrivial contribution $\Gamma^{(1)}W_j=-g_H W_k^* W_l^*$ with $j,k,l=1,2,3$ cyclic. The coefficient belonging to the resonance among critical modes is given by

$$g_H=\frac{2}{g_L}\langle \vec{v}_{K_c}|\mathcal{M}_0^c\vec{\mathcal{N}}_1(\vec{u}_{K_c}^{(1)}|\vec{u}_{K_c}^{(1)})-\vec{\mathcal{M}}_1^c(\vec{p}_{K_c}^{(1)}|\vec{u}_{K_c}^{(1)})\rangle, \quad (33)$$

so that now $V_j=2W_k^* W_l^*$. For PR 2WM with $R=1$ and $D=0$ the quadratic coefficient is calculated to be $g_H\approx -13.94$, so the H^π branch bifurcates subcritically. The eigenfunction $\vec{u}^{(2)}$ that modifies the longitudinal behavior is of the form

$$\vec{u}^{(2)}(z,K_c)=\rho\mu\vec{u}^{(1)}(z,K_c)+\vec{S}^{(2)}(z,K_c). \quad (34)$$

Here the Fredholm alternative introduces a second arbitrary factor ρ, which must not be rescaled by μ, for reasons to be discussed in Sec. V C.

In the second order, the resonant nonlinear-mode interaction cannot stabilize linear exponential growth, as it was also pointed out in Ref. [36], and the asymptotic expansion has to be carried out to third order. In this manner one obtains amplitude equations for the hexagonal pattern, which have the universal form

$$\tau_0\partial_t W_1=(\Gamma-\Gamma_c)W_1-g_\pi|W_1|^2W_1+g_H W_2^* W_3^* -g_{\pi/3}(|W_2|^2+|W_3|^2)W_1, \quad (35)$$

and analogously for W_2 and W_3 through the cyclic permutation of indices. These are the well-known coupled Landau hexagon equations with the hexagonal cross-coupling coefficient in the cubic order

$$g_{\pi/3}=\frac{g_H}{g_L}(\langle\vec{v}_{K_c}|\tilde{\mathcal{M}}_0\mathcal{N}_0-\tilde{\mathcal{L}}|\vec{u}^{(2)}_{K_c}\rangle+\langle\vec{v}_{K_c}|\tilde{\mathcal{M}}_0\vec{\mathcal{N}}_1(\vec{u}^{(1)}_{K_c}|\vec{u}^{(1)}_{K_c})-\vec{\tilde{\mathcal{M}}}_1(\vec{p}^{(1)}_{K_c}|\vec{u}^{(1)}_{K_c}))\rangle)+\frac{1}{g_L}\langle\vec{v}_{K_c}|\vec{m}_{\pi/3}-\mathcal{M}^c_0\vec{n}_{\pi/3}\rangle. \quad (36)$$

It consists of two parts $g_{\pi/3}=g^0_{\pi/3}-\rho\mu g_H$, as a consequence of Eq. (34), and is in whole proportional to μ^2. Here $g^0_{\pi/3}$ denotes the the part of the cubic cross-coupling coefficient for which $\rho=0$.

Besides the homogeneous state and stripe patterns, the coupled Landau hexagon equations [Eq. (35)] possess as a stationary solution a regular hexagon with the amplitude [15]

$$|W_1|=|W_2|=|W_3|=\frac{(-1)^n g_H\pm\sqrt{g_H^2+4G(\Gamma-\Gamma_c)}}{2G}, \quad (37)$$

where $G=g_\pi+2g_{\pi/3}$. Since the phases are not arbitrary here, and their sum must fulfill $\Psi=\psi_1+\psi_2+\psi_3=n\pi$, one distinguishes the positive hexagons (H^0) with integer n even, and the inverted haxagons (H^π) with n odd. The states with discrete total phase Ψ belong to the so-called phason modes. They arise for planforms with $2N\geqslant 5$ [17].

C. Stability and coexistence of photorefractive planforms

From the coefficients of bimodal and trimodal interaction that were calculated in the previous sections [Fig. 5(a)], we are now able to determine analytically the stability of planforms with any N-modal structure occurring in the PR feedback system. We consider the situation where the system develops almost perfect patterns and restrict the stability analysis of Landau equations to spatially homogeneous perturbations (see, e.g., [17,18]). Among the patterns with $N=2$ one generically finds that the stripes are stable if $g_\theta>g_\pi$, whereas the rhombi become stable if $g_\theta<g_\pi$. For the PR system considered here, in particular, the square pattern ($\theta=\pi/2$) is stable with respect to the stripes, and narrow rhombi (with $\theta=\pi/6$) are unstable. They both bifurcate supercritically. In general, a stripe pattern can never be stable in the parameter region of a system permitting a stable square pattern, because there exists no separatrix solution. For the hexagonal patterns ($N=3$), only the subcritical branch shows stable solutions. For the PR system we have $g_{\pi/3}>g_\pi$ and the stripes become stable while the hexagons become unstable for some higher values of Γ. Within the framework of $N=3$ pairs this leads to the phenomenon of stripe-hexagon competition. As a consequence of the stability of the square pattern in the PR feedback system, we anticipate square-hexagon competition instead. In the following we determine its onset. To describe the coexistence of squares and hexagons, one must consider at least the interaction of $N=6$ mode pairs [Fig. 4(c)], given by the Landau dodecagon equations [17,19],

$$\tau_0\partial_t W_1=(\Gamma-\Gamma_c)W_1-g_\pi|W_1|^2W_1+g_HW_2^*W_3^*-g_{\pi/3}(|W_2|^2+|W_3|^2)W_1-g_{\pi/2}|W_4|^2W_1-g_{\pi/6}(|W_5|^2+|W_6|^2)W_1, \quad (38)$$

and analogously for W_2 and W_3, and

$$\tau_0\partial_t W_4=(\Gamma-\Gamma_c)W_4-g_\pi|W_4|^2W_4+g_HW_5^*W_6^*-g_{\pi/3}(|W_5|^2+|W_6|^2)W_4-g_{\pi/2}|W_1|^2W_4-g_{\pi/6}(|W_2|^2+|W_3|^2)W_4, \quad (39)$$

and analogously for W_5 and W_6. They contain two sets of hexagons rotated by an angle of $\pi/2$, and hence allow for the description of 12-fold quasiperiodic patterns and the competition of hexagons and squares. The coupling coefficients g_θ involved in this interaction can be immediately read from Fig. 5(a). Besides the square and the hexagon branches, whose amplitudes are given by Eqs. (30) and (37), there exists a branch of equilateral dodecagonal pattern with the amplitude

$$|W_1|=\cdots=|W_6|=\frac{(-1)^n g_H\pm\sqrt{g_H^2+4G_D(\Gamma-\Gamma_c)}}{2G_D}, \quad (40)$$

where $G_D=g_\pi+g_{\pi/2}+2g_{\pi/3}+2g_{\pi/6}$. We are interested in the stability for each of these three patterns, which are the only potentially stable stationary solutions. The stability of the general Landau dodecagon equations was obtained and discussed in previous works [17,52]. Here we discuss important results for the PR feedback system. We find that hexagons dominate near primary threshold but there exists a secondary threshold

$$\Gamma_{Sq}-\Gamma_c=g_H^2\frac{g_\pi+g_{\pi/2}}{(g_\pi-g_{\pi/3}+g_{\pi/2}-g_{\pi/6})^2} \quad (41)$$

with $\Gamma_{Sq}L\approx 6.78$, at which the squares become stable and coexist with the hexagons. Along this square-hexagon competition, a parameter region emerges starting at

$$\Gamma_D-\Gamma_c=\frac{1}{4}g_H^2\frac{3g_{\pi/2}-g_\pi-2g_{\pi/3}+6g_{\pi/6}}{(g_\pi+2g_{\pi/3}-g_{\pi/2}-2g_{\pi/6})^2}, \quad (42)$$

with $\Gamma_DL\approx 6.71$, in which a stable dodecagonal pattern appears, so that tristability is possible. The stability scenario of the stationary substructures of dodecagonal planforms is depicted in Fig. 5(b). Whether the squares or the dodecagons become stable first, depends sensitively on the values of the cross-coupling coefficients. The coexistence of squares and hexagons does not necessarily imply dodecagonal patterns, as the dodecagon branch might be completely unstable. One has to keep in mind, of course, that an asymptotic bifurcation analysis is qualitatively valid only until the next bifurcation occurs in the full nonlinear system. However, the model for PR 2WM with intensity-dependent relaxation time has proven rather robust against secondary phase instabilities,

e.g., and hence we expect the dodecagonal patterns to be present in this nonlinear optical-feedback system.

V. NUMERICAL RESULTS

Analytical bifurcation theory, presented so far, predicts the threshold for the onset of pattern formation and the occurrence of an unstable annulus of spatial frequencies from which nonlinear-mode interaction, in correspondence with the amplitude-equation formalism, creates a definite pattern possessing a finite number of spatial-mode amplitudes.

For almost a decade, extreme difficulties in the numerical integration of the full set of nonlinear two-wave mixing, Eqs. (1) and (2), based on the reflection-grating type of interaction in a bulk photorefractive medium, have caused a lack of numerical results for patterns appearing in two transverse dimensions. However, they are solely needed for comparison of theory with experimental observations, and to corroborate plenty of previously obtained analytical results. For mirror distances $D>0$ nonlinear bifurcation analysis quickly becomes extremely involved [36]. Similar difficulties may appear in the multiple-pattern region discovered in experiment [31].

Numerical simulations are performed using a beam-propagation method that has been developed earlier in Refs. [27,38] to display transverse patterns in one dimension (1D), and that is appropriately modified to account for 2D. The difficulties in numerical treatment arise from the counterpropagation of the beams under two-point boundary conditions in a spatially extended system. A relaxation-type integration scheme of second order was found necessary, whose convergence puts extensive requirements on the computer memory and execution time. For a brief outline of this numerical integration scheme see Appendix B.

In optics, contrary to most of the hydrodynamic and ferromagnetic systems, e.g., the beam profiles are constrained to a finite lateral extent. A laser beam typically has a Gaussian envelope and the corresponding aspect ratio is low. Because of that, in photorefractive wave mixing the spatiotemporal attractors obtained so far have not been shown to possess domain boundaries or front dynamics. A higher-aspect-ratio can be achieved if the beam is broadened, so that a plateau forms. To accomplish higher-aspect-ratio conditions for the simulations, we have chosen the incident envelope of the pump A_1 to have the shape of a hyper-Gaussian beam, while the incident envelope of A_2 is determined by what is reflected back from the mirror,

$$A_1(x,y,0,t)=A_1\exp[-(x^2+y^2)^n], \tag{43a}$$

$$A_2(x,y,L,t)=-\sqrt{R}(T_F)^{-1}\{\exp(i\phi_K)T_F[A_1(x,y,L,t)]\}, \tag{43b}$$

where n is the order of the hyper-Gaussian beam. Here we report the results for the case $n=4$ (Fig. 6), all simulations being done for $D=0$ and $R=1$ with the diffraction parameter $f=0.034$. This corresponds to an aspect ratio of about 20.

A numerical grid of 128×128 points in the transverse plane and 300 points along the propagation direction is taken. The maximal spatial frequency that can be resolved is $K_{max}w_0/2\pi\approx6.3$, which corresponds to about $4K_c$. It turns out that at least $3K_c$ is required for the spectrum to sufficiently saturate higher modes and to produce physically reasonable mode amplitudes.

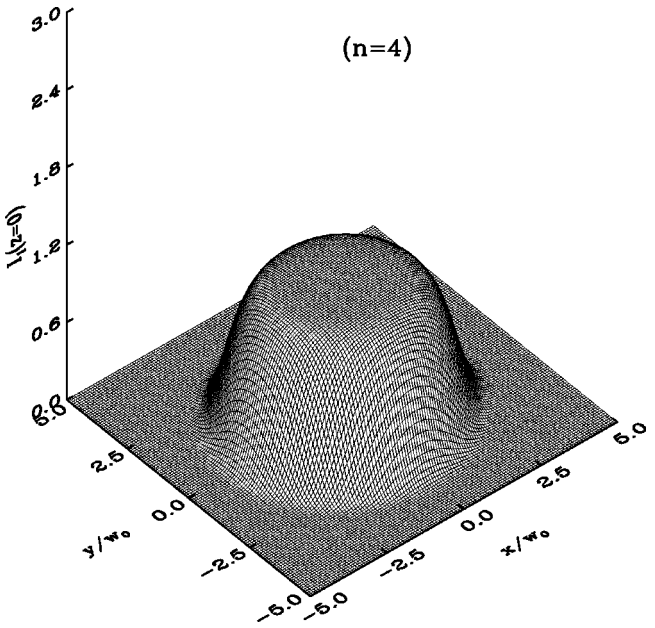

FIG. 6. Transverse intensity profile of beam I_1 as it enters the crystal at $z=0$ in the numerical grid of 128×128 points. The intensity is normalized to the intensity of the beam center.

A. Spontaneous hexagon formation

The broken inversion symmetry in the PR wave-mixing process causes the hexagonal structure to be the preferred pattern in the neighborhood of the primary threshold. Adiabatically approaching the instability threshold from below, for the value of the coupling strength very close to Γ_c, a hexagonal pattern spontaneously forms out of the initially homogeneous beam profile (Fig. 7). At $t=80\tau_{PR}$ a linearly unstable annulus of active modes becomes visible in the optical far field, although only very faint as compared to the pump beam. The nonlinear-mode interaction causes a breakup of this annulus into a structure of six beanlike spots, which eventually grow to form the hexagon, and the higher harmonic modes $\sqrt{3}K_c$ and $2K_c$ appear. This confirms recent experimental observations of the temporal evolution towards the hexagon state [28]. In the near field, at the output faces of the crystal, one immediately recognizes that the hexagonal patterns occur with opposite phases, i.e., at $z=0$ the inverted hexagons with the total phase $\Psi=\pi$ form, whereas at $z=L$ the positive hexagons with $\Psi=0$ are visible. This antiphase behavior is a characteristic feature of PR patterns and has been reported earlier for one-dimensional structures [38], where it led to stripelike modulations at the opposite faces of the crystal, which were spatially shifted with respect to each other because of the translational invariance. However, hexagons possess an intensity profile with broken inversion sym-

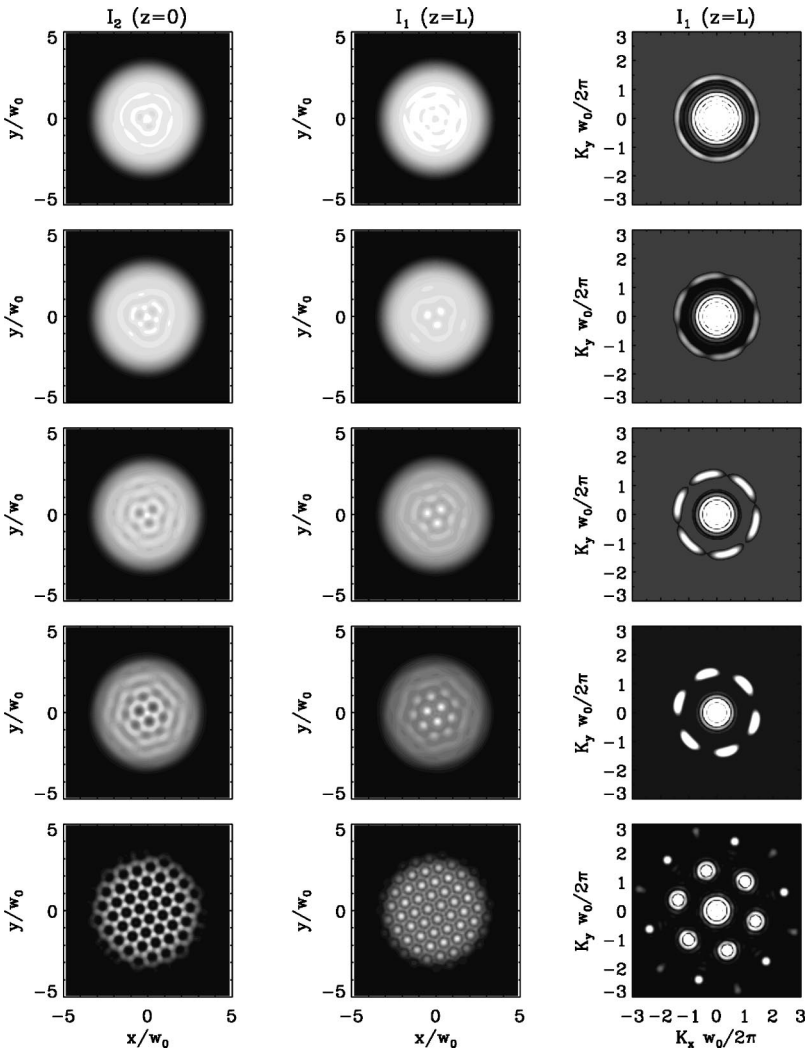

FIG. 7. Temporal evolution of transverse-beam profiles, depicting the development of a hexagonal structure out of the homogeneous state for $\Gamma L=3.9$, $R=1$, and $D=0$. Near-field pattern of the amplified beam $I_2(z=0)$ (left column), near-field pattern of the depleted beam $I_1(z=L)$ (middle column), and the spatial Fourier spectrum in the far field of the beam $I_1(z=L)$ (right column) are presented at different instances of time. Upper to lower row: transient patterns at $t/\tau_{PR}=80,240,360,440$ and the attractor at $t/\tau_{PR}=2000$. The contour levels of the far-field patterns have been chosen differently to clearly display the mode structure, and as a consequence the brightness of the pump beam may vary.

metry, and the antiphase behavior immediately results in the simultaneous appearance of the two different types of hexagons at the two output faces.

Before we discuss this phenomenon in more detail, let us present the temporal evolution into the hexagonal pattern, where this time a delta-peak-like perturbation of the refractive index is applied in the middle of the crystal to excite the active modes more strongly. For the coupling strength $\Gamma L=3.9$ we obtain the same transient behavior as in Fig. 7, however, for a value of $\Gamma L=4.0$ the transient is rather different (Fig. 8).

Despite the uniform perturbation in K space, a squarelike modulation emerges on the top of the annulus. Each of its stripelike substructures gives rise to a hexagonal substructure. The two hexagons are rotated by $\pi/2$ and form a dodecagonal structure. Since the dodecagon is unstable in this region of parameter space [cf. Fig. 5(b)], the two hexagonal substructures start competing with each other, leading to the formation and the long dynamics of penta-hepta defects. Eventually, all defects reach the edge of the beam profile and disappear, and in the steady state again a regular hexagon forms.

The intensity dependence of τ has no influence on the steady state, and does not change qualitatively our results close to the stationary primary-instability point. It may affect the slow temporal evolution of transient patterns. However, as shown for the temporal evolution of transverse modulations in 1D [38,53], the transient dynamics indeed becomes slower by two orders of magnitude, but without affecting the transverse shape of primary modulations. Traveling waves caused by the secondary instabilities were shown to possess much higher thresholds or may even be altogether impeded. This should make the predicted square-hexagon competetion more likely to be observable.

B. Longitudinal-mode propagation

In the following we discuss the longitudinal propagation of transverse modes through the PR medium. As mentioned above, an antiphase behavior of transverse patterns is present. It originates from the longitudinal propagation of the pattern within a bulk nonlinear medium. The eigenfunctions that describe the longitudinal propagation of each transverse mode have been calculated analytically from the linear spectrum of the corresponding eigenfunctions using the amplitude-equation formalism in Sec. IV B. We will focus on the propagation of the two lowest-order modes: the critical mode K_c and the first higher-order mode $\sqrt{3}K_c$ of a hexagon.

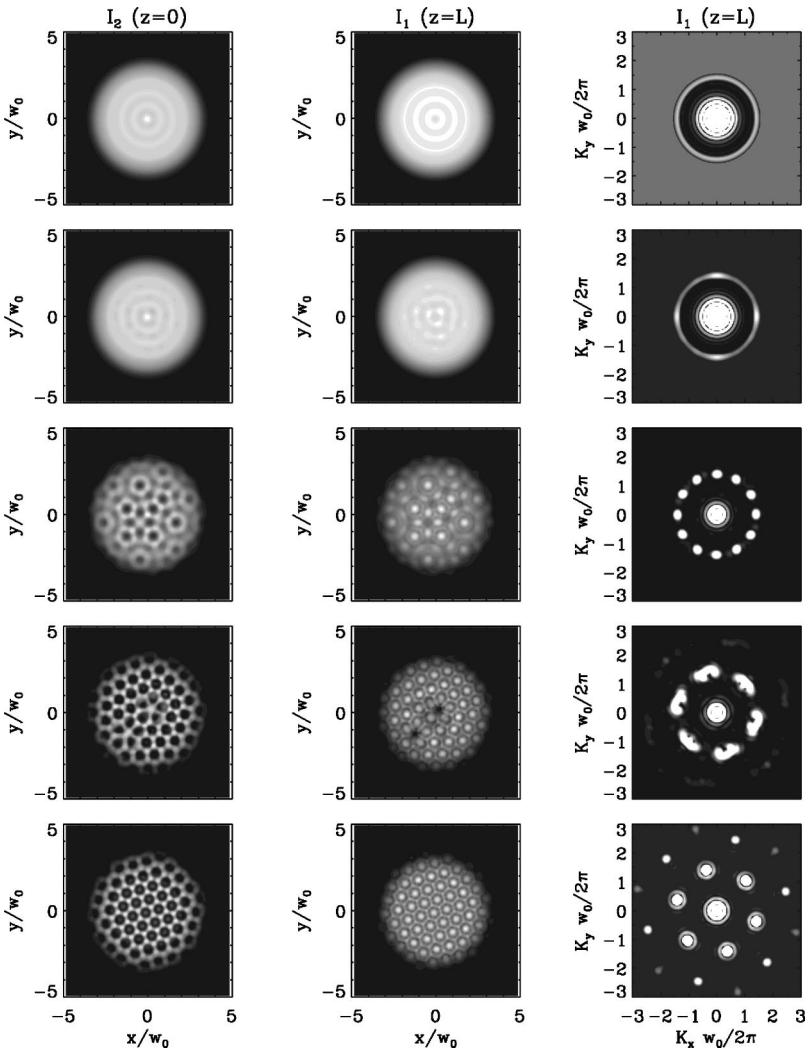

FIG. 8. Temporal evolution of transverse-beam profiles depicting the development of a hexagonal structure out of the homogeneous state for $\Gamma L=4.0$, $R=1$, and $D=0$. The notation is as in Fig. 7, except that the transient patterns are shown for $t/\tau_{PR}=300,500,700,1600$ and the attractor for $t/\tau_{PR}=5000$. The development of defect pairs is clearly visible.

The spatial modes from numerical data are localized in the near field and have a broadened spot size in the optical far field. Therefore, their mode amplitudes are taken as the amplitudes of the envelope of the wave packet. In performing the analytical treatment we assumed the homogeneous fixed-point solution to be infinitely extended in the transverse direction, i.e., we restricted the analysis to an infinitely high aspect ratio. As a consequence one should encounter discrepancies that become more prominent as the aspect ratio is lowered, or as less modulations occur compared to the unmodulated beam envelope [54]. The hyper-Gaussian beam profile approximates the assumption of an infinitely extended modulation from the analysis more closely, and the discrepancies remain rather small.

Figure 9 compares the analytical eigenfunctions to the results obtained from the numerical simulations. All eigenfunctions have been normalized to $\mathrm{Re}\, a_2(z=0,K_c)=1$ for better comparison. As a consequence of the nature of the first-order phase transition and the fact that the stable solution only comes with very large amplitude, there are noticeable deviations in the propagation of the real and imaginary parts of eigenmodes from the analytical prediction for different values of Γ on the hexagon branch. The best agreement is found for $\Gamma L=3.32$ at the lower hysteresis point. The phase between the pump and the sideband beams (carried by the eigenfunction) rotates with an increasing bifurcation parameter Γ. To circumvent this problem we choose $|a_2(z=0,K_c)|=1$ for normalization, to extract the hexagon and stripe amplitudes plotted in Fig. 10. This choice, however, will yield coefficients that are quantitatively meaningless without the explicit knowledge of the eigenfunction at the place where the pattern is observed.

The development of transverse structures through the crystal can be viewed in a more physical manner by looking at the light-intensity modulation $\delta I_{1,2}$ [Figs. 9(c) and 9(f)]. The intensity profiles have to be taken with caution though, when used for displaying the development of a specific mode because in calculating intensities different spatial modes might mix. Starting from the unmodulated input profile, there are regions where the modulation is positive, i.e., the intensity in the beam center is maximal and the corresponding pattern phase is $\Psi=0$. For the backward-propagating beam there is a region where the modulation is negative and the pattern phase is $\Psi=\pi$. This is the origin of the antiphase behavior of patterns at the opposite output faces of the crystal. The mode $\sqrt{3}K_c$ displays nodes at the propagation distances z where its amplitude vanishes. The combination of all

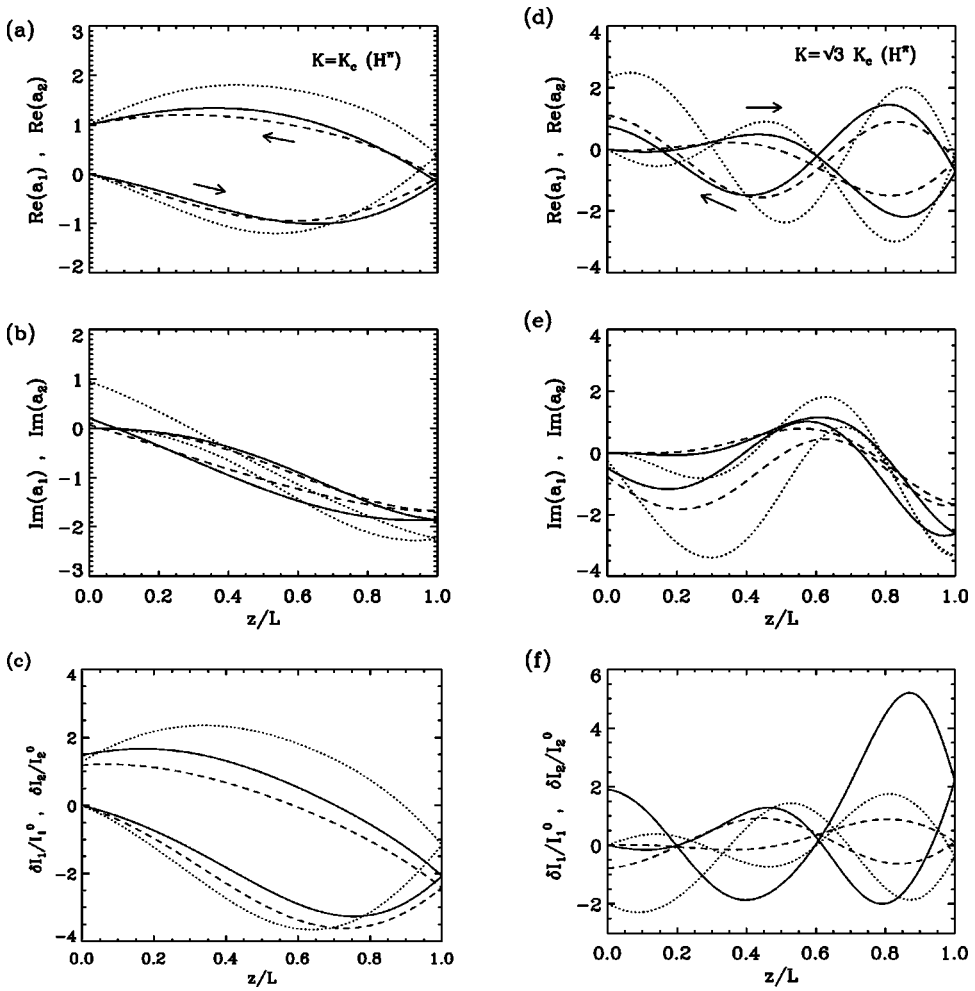

FIG. 9. Longitudinal propagation of transverse modes. Analytical eigenfunctions (solid lines) and numerical eigenfunctions for $\Gamma L = 3.32$ (dashed) and $\Gamma L = 3.80$ (dotted) are presented. (a) Real and (b) imaginary parts, and (c) relative intensity modulation of the hexagon mode K_c. (d)–(f) The same for the hexagon mode $\sqrt{3}K_c$. Each plot depicts both the forward- and backward-propagating beams indicated by arrows.

tranverse modes with their different mode amplitudes forms the series of intensity patterns, as in Fig. 11. Two lateral cuts through the intensity profile $I_2(z=0)$ of Fig. 11(d) across the x and y direction, respectively, reveal a large spatial modulation of the amplitude, as a consequence of the first-order phase transition. Locally the intensity rises almost three times above the homogeneous background [Fig. 12(a)]. Such

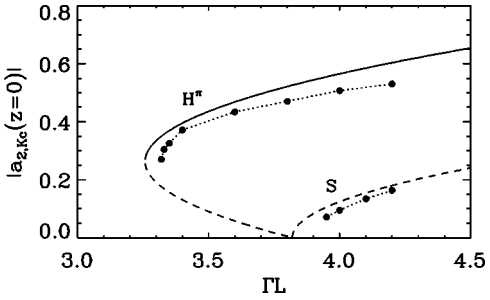

FIG. 10. Amplitude of the modulated structure for one spot pair of the critical mode K_c as a function of the coupling strength in the case of inverted hexagons (H^π) and stripes (S). Solid (dashed) line denotes the stable (unstable) branches obtained by the amplitude equations for the self-organized structures. The normalization factor is $\mu = \mu_m^{(1)} \approx 0.0476$. Results from the numerical simulations of self-organized hexagons and of the Fourier-controlled stripes are represented by bullets. The dotted lines are a guide for the eye.

a large pattern amplitude indicates that a strong renormalization for the asymptotic expansion is present.

C. Subcritical hexagons and strong renormalization

From the discussion in the previous section it is clear that the absolute value of the order parameter W, given by the amplitude equation, loses its physical meaning without the explicit knowledge of the longitudinal eigenfunction $\vec{u}(z)$ in the bulk medium. Moreover, the critical-mode amplitude a_{K_c} and the pattern amplitude a must clearly be distinguished, as they certainly coincide only very close to the threshold. The pattern amplitude is a superposition of the order parameters multiplied by the eigenfunctions at the propagation position z where the pattern is observed. However, the mode amplitudes obtained from the analysis can still give rather accurate results even far away from the threshold, depending on how strong the renormalization of the longitudinal behavior is and how many higher orders have to be taken into account.

The first-order phase transition of hexagons is accompanied by a large pattern amplitude near the bifurcation point, hence a strong renormalization of the eigenfunction $\vec{u}(z,K_c)$ is anticipated. In the following we determine the strength of the renormalization according to our multiple-scale expansion. Assuming that the hexagon has the form as in Fig.

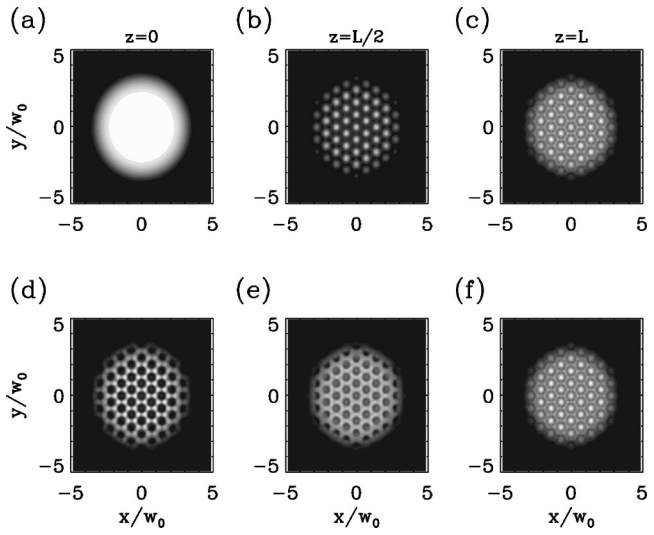

FIG. 11. Transverse patterns of the light field of the forward-propagating beam I_1 (a)–(c) and of the backward-propagating beam I_2 (d)–(f) at different positions within the crystal: $z=0$ (a) and (d), $z=L/2$ (b) and (e) and $z=L$ (c) and (f). $\Gamma L=3.8$ slightly below the bifurcation point.

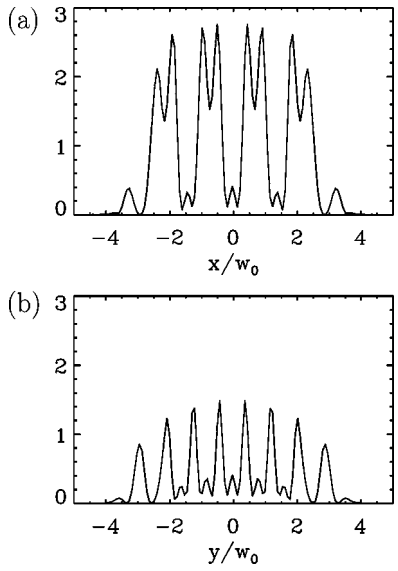

FIG. 12. Cuts through the transverse-intensity profiles of the beam $I_2(z=0)$, as in Fig. 11(d). (a) Cut along $y=0$ and (b) cut along $x=0$ in the direction of one K vector. Intensities are normalized to the input beam intensity $I_1(x,y,z=0)$.

11(d), the amplitudes equal $|W^H|$ and the phases obey $\psi_1=\psi_2=\psi_3=\psi^H=\pi$. Combining the expansion ansatz (14c) with Eqs. (31) and (22), the amplitude of the hexagon at the beam center is given by

$$a_{2,K_c}(0,0,z)=3[r_3^{(1)}(z)|W^H|\cos(\psi^H) + 2r_3^{(2)}(z)|W^H|^2\cos(2\psi^H)] + (\text{higher-order terms}). \tag{44}$$

$$=3\left[r_3^{(1)}(z) + \frac{2g_H}{G}r_3^{(2)}(z)\right]|W^H|\cos(\psi^H) + 6\frac{\Gamma-\Gamma_c}{G}r_3^{(2)}(z) + (\text{higher-order terms}) \tag{45}$$

$$\approx 3r_3^{(tot)}(z)|W^H|\cos(\psi^H), \tag{46}$$

where $r_3(z,K_c)$ is the third component of the eigenfunction in the untransformed basis, and where the term proportional to $(\Gamma-\Gamma_c)/G$ is negligible up to this order. Renormalization of the total eigenfunction according to $\mathrm{Re}\, r_3^{(tot)}(z=0)=1$ will modify the normalization factor. It can be expressed as the product of the normalization factors at each order. In our case $\mu=\mu^{(1)}\mu^{(2)}$, where the factor at second order reads as

$$\mu^{(2)}=\frac{1+\eta_c\rho\mu^{(1)}}{1-\eta_c\,\mathrm{Re}\,\tilde{S}_3^{(2)}(0)}, \tag{47}$$

with the critical ratio $\eta_c=2(-1)^n g_H/G^0$, and $\tilde{S}_3^{(2)}$ is the inhomogeneous part of Eq. (34) in the untransformed basis. If a strong renormalization factor is found $\mu^{(2)}\neq 1$, it leads to discrepancies between the critical-mode amplitude and the order-parameter. This phenomenon is related to the subcriticality dilemma, arising in the asymptotic expansion to obtain Landau equations for a first-order phase transition, where subsequent orders become comparable and η_c is of the order of one. However, for order-parameter equations like Eq. (35) or Eqs. (38) and (39) to be still a valid approximation, the normalization must be unique for all planforms, simultaneously. Consequently, we have chosen $\mu=\mu^{(1)}$ such that the eigenfunctions for the rhombi are normalized, and $\mu^{(2)}$ now becomes a scaling factor due to the renormalization of the hexagons. As mentioned above, for hexagons it is necessary to normalize the moduli of amplitudes, because the phase of the eigenfunction rotates with increasing bifurcation parameter. Therefore, the hexagon-mode amplitude in Fig. 10 is related to the order parameter from Fig. 5(b) by

$$|a_{2,K_c}(z=0)|=\frac{1}{\mu_m^{(2)}}\frac{\mu^{(1)}}{\mu_m^{(1)}}|W_1|, \tag{48}$$

where μ_m denotes the normalization for the moduli. This yields a scaling factor due to renormalization of $\mu_m^{(2)}\approx 0.4$, and a strong renormalization indeed occurs.

If the renormalization was weak, the free parameter ρ [cf. below Eq. (36)] could be chosen arbitrarily, e.g., according to an orthogonality condition, because then $\mu^{(2)}$ and $g_{\pi/3}$ would be nearly independent of ρ. This, however, is not the case here and $g_{\pi/3}$ strongly depends on the choice of ρ. We decided to determine its value by a fit of the analytical curve to our numerical results in such a way that the ratio of g_H and $g_{\pi/3}$ yields the same hysteresis, taking into account that be-

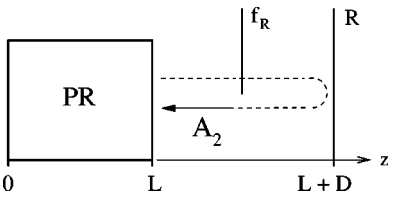

FIG. 13. Geometry of the feedback loop supplied with the filter mask f_R placed in the Fourier plane.

cause of the low aspect ratio of patterns, the amplitudes from numerics always lie somewhat below the analytical values. In this manner $\rho=7.30$ and we obtain $g_{\pi/3}=35.38$. This procedure is, of course, unsatisfactory from a theoretical point of view. The question of how to determine ρ in an analytically consistent way may only be answered if the multiple-scale expansion is carried out to higher orders.

VI. FOURIER SELECTION

Both our analytical calculations and numerical simulations have shown that close to the primary threshold, the hexagonal pattern is the only stable structure when $D=0$ and $R=1$. But it also has become clear that a majority of patterns, in fact any regular array of $2N$ spots out of the annulus of active modes, exists as an unstable stationary solution. It is now desirable to have an access to these structures and manipulate the system to select and stabilize the unstable states [39]. Such an approach provides us, on one hand, with access to the whole set of possible pattern states, and on the other hand, with a broader insight into the underlying mechanisms in the process of pattern formation in a bulk PR medium.

Motivated by the Fourier-filtering technique that has been used in experiments so far [49], we use the same filtering technique and study its impact on this pattern-forming system. A Fourier-filter mask $f_R(K_x,K_y)$ is inserted into the feedback path (Fig. 13) to manipulate the mirror boundary conditions for certain spatial modes, which we want to suppress. It is important to note that the pump beam must not be disturbed in any way. Black areas in the filter mask absorb all spatial components, and thus are equivalent to a zero boundary condition for the modes K such that $a_{2,K}(z=L)=0$. Undoubtedly, the method is strongly invasive, as it alters the boundary conditions and hereby switches some of the active modes to passive ones. So, one may expect not to be able to stabilize unstable eigenstates of the filterless system in this way.

Figures 14 and 15 display the stripe and square patterns that are successfully selected by applying the corresponding Fourier masks presented in Figs. 16(a) and 16(b). In the near field both patterns again show the typical antiphase behavior characteristic of PR pattern formation. Despite the invasive filtering, the stripe pattern completely coincides with the unstable stripe solution of the filterless system. Both its amplitude from Fig. 10 and its longitudinal eigenfunction [Figs. 17(a) and 17(b)] are in good agreement with the analytical curves calculated for the originally unstable stripe state.

When the Fourier filtering is applied to the case of

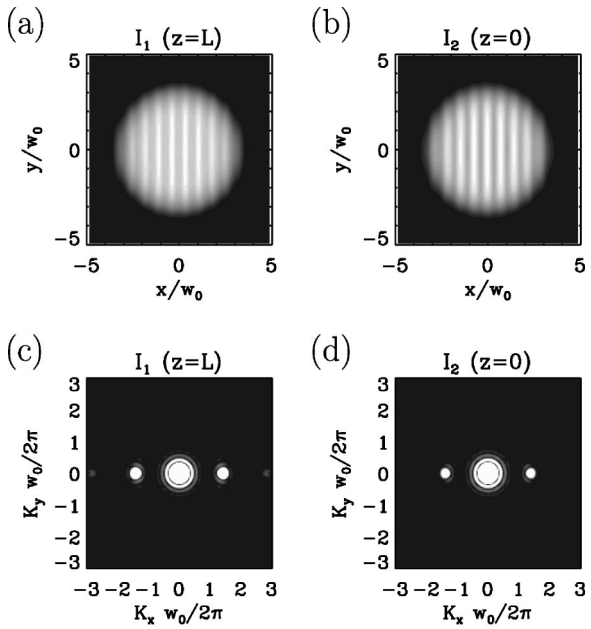

FIG. 14. Stripe pattern for $\Gamma L=4.1$ when the slit filter mask is present in the feedback loop. (a) Near-field pattern of the depleted and (b) of the amplified beam. (c) and (d) are the corresponding far-field patterns.

squares, the lowest-order interaction modes $K_{\pm}=\sqrt{2}K_c$, among other higher-order modes, are blocked by the choice of the filter mask. However, this does not mean that the higher harmonic modes remain zero throughout the crystal. From Figs. 17(d) and 17(e) it is seen that the nonlinear bulk medium tends to recover the form of the longitudinal-propagation mode. The propagation of the critical mode K_c of the square pattern is not affected by the lack of the interaction modes. Nevertheless, higher harmonic modes are es-

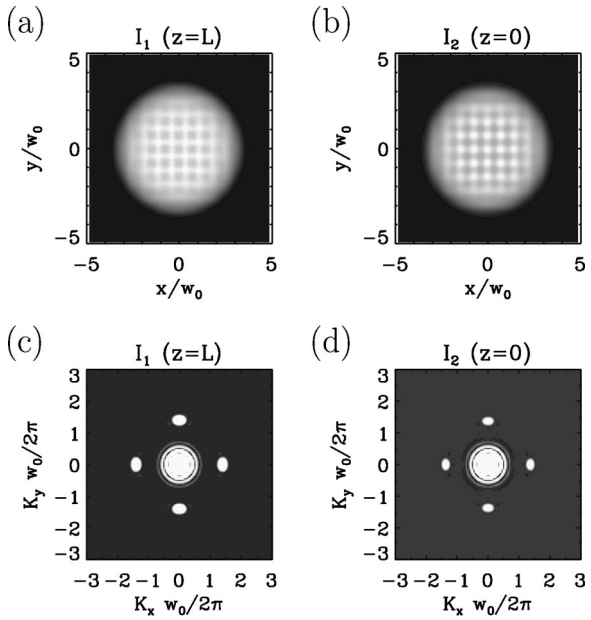

FIG. 15. Square pattern for $\Gamma L=4.1$ when the cross-filter mask is present in the feedback loop. Notation is the same as in Fig. 14.

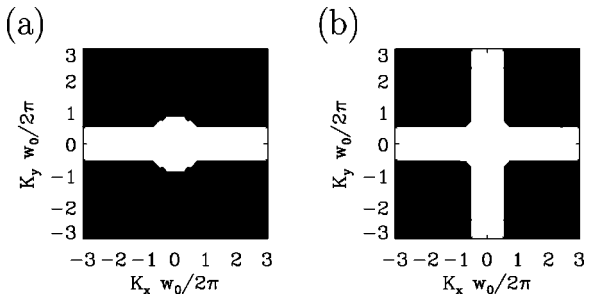

FIG. 16. Spatial Fourier-filter masks $f_R(K_x,K_y)$. (a) Slit and (b) cross filter.

sential constituents of the desired pattern and should not be suppressed by the filter, thus a more careful choice of masks is required as it is noted in Ref. [39].

Even though we are using an invasive filtering technique, an important feature of the self-organization process can be inferred from it. When the stripes have been selected and they reach steady state, replacing the slit filter by the cross filter will make the squares appear. The fact that the squares can be selected in this way at all is a direct consequence of the stability of the square pattern. Within the subsystem defined by the filter, the squares are stable with respect to the stripes [cf. Fig. 5(a)]. Furthermore, the invasive filtering method provides an important indication for the square-hexagon competition in the PR feedback system in the parameter region considered.

If the stripe solution was selected in either of the two perpendicular directions of the cross filter, it would be a strong indication for the effect of stripe-hexagon competition rather than square-hexagon competition. But obviously, that is not the case.

VII. CONCLUSIONS

The present paper, for the first time to our knowledge since the initial experimental observations, presents numerical simulations of two-dimensional patterns in a bulk photorefractive crystal with a single feedback mirror. Thus far energy transfer between two beams and the interaction via reflection gratings in a spatially extended system have precluded simulations of the full set of nonlinear wave-mixing equations. With our relaxation-type integration scheme we are able to study the spontaneous formation of two-dimensional structures in the transverse-beam profiles, their longitudinal development within the nonlinear optical crystal, and the effects of Fourier filtering on the mode-selection process.

In the self-organization process hexagons are identified as the predominant patterns above the primary instability threshold. The longitudinal variation of the wave-mixing process, through the change in the refractive index, causes the breaking of the inversion symmetry. Out of the homogeneous beam profile the faint annulus of transverse modes develops in the first stage. For weak initial perturbations

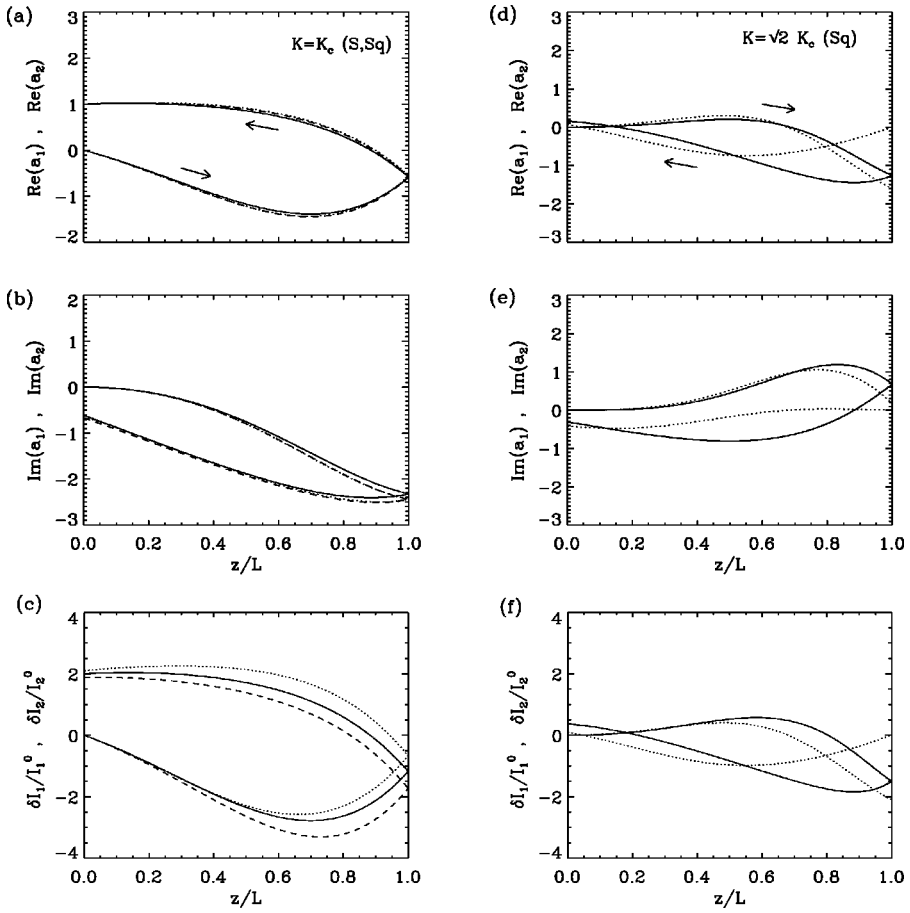

FIG. 17. Longitudinal propagation of transverse modes in the geometry with filter. Analytical eigenfunctions (solid lines) and numerical eigenfunctions with $\Gamma L=4.0$ for stripes (dashed) and squares (dotted) are displayed. (a) Real and (b) imaginary parts and (c) relative intensity modulation of critical mode K_c. (d)–(f) The same for the square mode $\sqrt{2}K_c$. Each plot depicts the forward- and backward-propagating beams indicated by arrows.

hexagons then immediately arise through the breakup of this unstable annulus. They appear through a subcritical bifurcation with a prominent hysteresis and a large amplitude. In the PR pattern formation an antiphase behavior is observed, which results in the simultaneous appearance of the positive and inverted hexagons at the opposite output faces of the crystal. Penta-hepta defects may cause a long transient dynamics, but eventually they disappear at the edges of the beam profiles.

The linear instability threshold and the angle of the sideband beams turn out to be very robust against the reduction of mirror reflectivity. Whether stationary or oscillatory instabilities occur depends strongly on the model for the photorefractive time constant. The typical inverse intensity dependence of the relaxation time leads to the correct prediction of stationary patterns for real mirror distances, in accordance with the experiments.

The stability and coexistence of planforms has been determined by a multiple-scale analysis, leading to the coupled Landau equations for any *N*-modal structures. The cubic self- and cross-coupling coefficients for a mirror with high reflectivity placed at the exit face of the crystal have been calculated, carefully incorporating and discussing the normalization of longitudinal eigenfunctions for a quantitative comparison with our numerical results, including eigenfunctions of higher-order modes.

For an array of six spot pairs the nonlinear bifurcation analysis predicts the occurrence of square-hexagon competition rather than the stripe-hexagon competition and, moreover, a parameter region where a stable dodecagonal pattern should be observable in the PR feedback system. Because of the extreme computational requirements this could not yet be confirmed by our numerical-integration procedure.

Along with the first-order phase transition, a strong renormalization factor has been determined for the hexagonal-mode interaction. Hence the hexagon amplitude considerably deviates from the order parameter obtained by the Landau equations. This phenomenon is related to the subcriticality dilemma here, for example, occurring for the hexagonal-mode interaction, which arises in the asymptotic expansion if subsequent orders become comparable. Regardless of the order (cubic or higher) of the expansion, one must always ensure that normalization is unique for all planforms simultaneously.

An invasive Fourier-filtering method has been used to select stripes and squares that are otherwise unstable solutions. For wave mixing in a bulk medium the filter mask changes the boundary conditions for certain modes and tends to suppress them. However, the finite medium partly recovers the propagation of these modes and the squares could be successfully selected by a cross-shaped filter. Yet, the invasive Fourier filtering may provide deeper insight into the pattern-formation processes of the filterless system, as an indicator of square-hexagon competition, e.g. Although the stripe pattern obtained with a filter completely coincides with the unstable stripe state without filter calculated from the nonlinear analysis, one should not yet speak of pattern control in this context, in the sense that unstable eigensolutions have been stabilized. It remains to be seen by means of a more rigorous theoretical proof, whether a static manipulation method is capable of stabilizing unstable eigenpatterns in the feedback system within a nonlinear bulk photorefractive medium.

APPENDIX A: VECTORS AND MATRICES OF NONLINEAR INTERACTION

In the following we present the details of the field-grating and nonlinear-mode interaction involved in the multiple-scale anlysis to obtain the amplitude equations for pattern formation in PR wave mixing. The general form of the wave-mixing equations (13), listed here again for completeness,

$$\mathcal{L}_{z;x,y}\vec{U}+\mathcal{M}_0\vec{P}=\vec{\mathcal{M}}_1(\vec{P}|\vec{U}), \tag{A1a}$$

$$[\mathcal{D}_{0,t}+\mathcal{D}_{1,t}(\vec{U})+\mathcal{D}_{2,t}(\vec{U}|\vec{U})+\cdots]\vec{P}-\mathcal{N}_0\vec{U} =\vec{\mathcal{N}}_1(\vec{U}|\vec{U})+\vec{\mathcal{N}}_2(\vec{U}|\vec{U}|\vec{U})+\cdots, \tag{A1b}$$

presents the starting point of our expansion procedure, where we follow an idea by Geddes *et al.* [11]. The idea is conceived for wave mixing in Kerr media, and needs to be modified to be applicable to the grating dynamics occuring in PR wave mixing with slow medium response. Equations (A1) are obtained from Eqs. (12) by a basis transformation from the complex vectors of deviations to a real (4+2)-dimensional vector space,

$$\begin{pmatrix} U_1 \\ U_2 \\ U_3 \\ U_4 \end{pmatrix} = \begin{pmatrix} 1 & 1 & -1 & -1 \\ -i & i & -i & i \\ 1 & 1 & 1 & 1 \\ -i & i & i & -i \end{pmatrix} \begin{pmatrix} a_1 \\ a_1^* \\ a_2 \\ a_2^* \end{pmatrix}, \tag{A2a}$$

$$\begin{pmatrix} P_1 \\ P_2 \end{pmatrix} = \begin{pmatrix} 1 & 1 \\ -i & i \end{pmatrix} \begin{pmatrix} q \\ q^* \end{pmatrix}. \tag{A2b}$$

We prefer the (4+2)-dimensional to the six-dimensional vector space used by Lushnikov [36], because the grating variables can be eliminated at each order of the expansion, and one is left with a four-dimensional problem, instead.

Equations (A1) are general in the sense that they describe the behavior of wave mixing independent of whether the interactions of field and grating variables originate from two- or four-wave mixing, and they apply to both the stationary and oscillatory instabilities.

The notations $(\vec{U}|\vec{U})$ and $(\vec{U}|\vec{U}|\vec{U})$ denote the products of different quadratic and cubic nonlinearities. In the case of PR two-wave mixing discussed in the text, the general interaction matrices and vectors are given for the case $R=1$. The spatial- and temporal-derivative operators are

$$\mathcal{L}_{z;x,y} = \begin{pmatrix} \partial_z-\Gamma & -f\nabla_\perp^2 & 0 & 0 \\ f\nabla_\perp^2 & \partial_z & 0 & 0 \\ 0 & 0 & \partial_z & -f\nabla_\perp^2 \\ 0 & 0 & f\nabla_\perp^2 & \partial_z-\Gamma \end{pmatrix}, \tag{A3}$$

$$\mathcal{D}_{0,t}=\tau(I^0)\partial_t+1, \tag{A4}$$

$$\mathcal{D}_{1,t}=-\frac{\kappa}{2}\tau(I^0)U_3\partial_t, \tag{A5}$$

$$\mathcal{D}_{2,t}=-\frac{\kappa}{16}\tau(I^0)[U_1^2+U_2^2-3U_3^2+U_4^2-2(\kappa-1)U_3^2]\partial_t, \tag{A6}$$

where the matrices $\mathcal{D}_{j,t}$ have been reduced to scalar operators because $\tau(I^0)$ is real valued. The linear coupling matrices read as

$$\mathcal{M}_0=\Gamma\begin{pmatrix}0&0\\0&0\\1&0\\0&1\end{pmatrix}, \tag{A7}$$

$$\mathcal{N}_0=\begin{pmatrix}0&0&0&0\\0&0&0&1\end{pmatrix} \tag{A8}$$

and the nonlinear field-field and field-grating coupling results in the vectors

$$\vec{\mathcal{M}}_1=\frac{\Gamma}{4}\begin{pmatrix}P_1&P_2&0&0\\P_2&-P_1&0&0\\0&0&-P_1&-P_2\\0&0&-P_2&P_1\end{pmatrix}\begin{pmatrix}U_1\\U_2\\U_3\\U_4\end{pmatrix}, \tag{A9}$$

$$\vec{\mathcal{N}}_1=-\frac{1}{4}\begin{pmatrix}U_1^2+U_4^2\\U_1U_2+U_3U_4\end{pmatrix}, \tag{A10}$$

$$\vec{\mathcal{N}}_2=\frac{1}{16}\begin{pmatrix}2U_3(U_1^2+U_4^2)\\2U_1U_2U_3-U_4(U_1^2+U_2^2-U_3^2+U_4^2)\end{pmatrix}. \tag{A11}$$

One recognizes that up to third order none of the nonlinear temporal derivatives contributes to the dynamics of the Landau equation. The nonlinear self-coupling coefficient g_π, given in Eq. (27), depends on the longitudinal eigenfunctions of the first and second order through

$$\vec{m}_\pi=2\vec{\mathcal{M}}_1^c(\vec{p}_{K_c}^{(1)}|\vec{u}_{K=0}^{(2)})+2\vec{\mathcal{M}}_1^c(\vec{p}_{K=0}^{(2)}|\vec{u}_{K_c}^{(1)})+\vec{\mathcal{M}}_1^c(\vec{p}_{K_c}^{(1)}|\vec{u}_{2K_c}^{(2)})+\vec{\mathcal{M}}_1^c(\vec{p}_{2K_c}^{(2)}|\vec{u}_{K_c}^{(1)}), \tag{A12}$$

$$\vec{n}_\pi=2\vec{\mathcal{N}}_1(\vec{u}_{K_c}^{(1)}|\vec{u}_{K=0}^{(2)})+2\vec{\mathcal{N}}_1(\vec{u}_{K=0}^{(2)}|\vec{u}_{K_c}^{(1)})+\vec{\mathcal{N}}_1(\vec{u}_{K_c}^{(1)}|\vec{u}_{2K_c}^{(2)})+\vec{\mathcal{N}}_1(\vec{u}_{2K_c}^{(2)}|\vec{u}_{K_c}^{(1)})+3\vec{\mathcal{N}}_2(\vec{u}_{K_c}^{(1)}|\vec{u}_{K_c}^{(1)}|\vec{u}_{K_c}^{(1)}); \tag{A13}$$

the rhombic cross-coupling coefficient g_θ, in Eq. (28), through

$$\vec{m}_\theta=2\vec{\mathcal{M}}_1^c(\vec{p}_{K_c}^{(1)}|\vec{u}_{K=0}^{(2)})+2\vec{\mathcal{M}}_1^c(\vec{p}_{K=0}^{(2)}|\vec{u}_{K_c}^{(1)})+2\vec{\mathcal{M}}_1^c(\vec{p}_{K_c}^{(1)}|\vec{u}_{K_+}^{(2)})+2\vec{\mathcal{M}}_1^c(\vec{p}_{K_+}^{(2)}|\vec{u}_{K_c}^{(1)})+2\vec{\mathcal{M}}_1^c(\vec{p}_{K_c}^{(1)}|\vec{u}_{K_-}^{(2)})+2\vec{\mathcal{M}}_1^c(\vec{p}_{K_-}^{(2)}|\vec{u}_{K_c}^{(1)}), \tag{A14}$$

$$\vec{n}_\theta=2\vec{\mathcal{N}}_1(\vec{u}_{K_c}^{(1)}|\vec{u}_{K=0}^{(2)})+2\vec{\mathcal{N}}_1(\vec{u}_{K=0}^{(2)}|\vec{u}_{K_c}^{(1)})+2\vec{\mathcal{N}}_1(\vec{u}_{K_c}^{(1)}|\vec{u}_{K_+}^{(2)})+2\vec{\mathcal{N}}_1(\vec{u}_{K_+}^{(2)}|\vec{u}_{K_c}^{(1)})+2\vec{\mathcal{N}}_1(\vec{u}_{K_c}^{(1)}|\vec{u}_{K_-}^{(2)})+2\vec{\mathcal{N}}_1(\vec{u}_{K_-}^{(2)}|\vec{u}_{K_c}^{(1)})+6\vec{\mathcal{N}}_2(\vec{u}_{K_c}^{(1)}|\vec{u}_{K_c}^{(1)}|\vec{u}_{K_c}^{(1)}), \tag{A15}$$

and the cubic hexagonal cross-coupling coefficient $g_{\pi/3}$, in Eq. (36), through

$$\vec{m}_{\pi/3}=2\vec{\mathcal{M}}_1^c(\vec{p}_{K_c}^{(1)}|\vec{u}_{K=0}^{(2)})+2\vec{\mathcal{M}}_1^c(\vec{p}_{K=0}^{(2)}|\vec{u}_{K_c}^{(1)})+2\vec{\mathcal{M}}_1^c(\vec{p}_{K_c}^{(1)}|\vec{u}_{K_c}^{(2)})+2\vec{\mathcal{M}}_1^c(\vec{p}_{K_c}^{(2)}|\vec{u}_{K_c}^{(1)})+2\vec{\mathcal{M}}_1^c(\vec{p}_{K_c}^{(1)}|\vec{u}_{\sqrt{3}K_c}^{(2)})+2\vec{\mathcal{M}}_1^c(\vec{p}_{\sqrt{3}K_c}^{(2)}|\vec{u}_{K_c}^{(1)}), \tag{A16}$$

$$\vec{n}_{\pi/3}=2\vec{\mathcal{N}}_1(\vec{u}_{K_c}^{(1)}|\vec{u}_{K=0}^{(2)})+2\vec{\mathcal{N}}_1(\vec{u}_{K=0}^{(2)}|\vec{u}_{K_c}^{(1)})+2\vec{\mathcal{N}}_1(\vec{u}_{K_c}^{(1)}|\vec{u}_{K_c}^{(2)})+2\vec{\mathcal{N}}_1(\vec{u}_{K_c}^{(2)}|\vec{u}_{K_c}^{(1)})+2\vec{\mathcal{N}}_1(\vec{u}_{K_c}^{(1)}|\vec{u}_{\sqrt{3}K_c}^{(2)})+2\vec{\mathcal{N}}_1(\vec{u}_{\sqrt{3}K_c}^{(2)}|\vec{u}_{K_c}^{(1)})+6\vec{\mathcal{N}}_2(\vec{u}_{K_c}^{(1)}|\vec{u}_{K_c}^{(1)}|\vec{u}_{K_c}^{(1)}), \tag{A17}$$

where the eigenfunctions of the grating in the second order are related to the field eigenfunctions by $\vec{p}_K^{(2)}(z)=\mathcal{N}_0\vec{u}_K^{(2)}(z)+\vec{\mathcal{N}}_1[\vec{u}_{K_c}^{(1)}(z)|\vec{u}_{K_c}^{(1)}(z)]$ for modes K.

The superscript c denotes that $\vec{\mathcal{M}}_1$ has to be taken with $\Gamma=\Gamma_c$ coming from the expansion in ϵ, which in this case reads $\vec{\mathcal{M}}_1=\vec{\mathcal{M}}_1^c+\epsilon\vec{\mathcal{M}}_1^{(1)}+\cdots$.

APPENDIX B: RELAXATION-TYPE BEAM-PROPAGATION METHOD

We briefly outline the numerical-integration scheme to solve the coupled nonlinear partial differential equations (1) and (2) under two-point boundary conditions [Eqs. (43)] in the case of a photorefractive nonlinearity including strong pump depletion. For the spatial problem in two transverse dimensions we apply a simple spectral method [55]. We consider one of the two propagation equations for the light fields, e.g., Eq. (1a),

$$(\partial_z-ifK^2)\tilde{A}_1(z)=-\widetilde{QA}_2(z), \tag{B1}$$

which has already been transformed into the Fourier space, where $K^2=K_x^2+K_y^2$. The tilde denotes the spatial Fourier transform achieved by use of a fast-Fourier-transform algo-

rithm. In Eq. (B1), only the dependence on the propagation variable z is retained. The initial partial differential equation is thus transformed into a system of ordinary differential equations, with as many equations as there are Fourier components. In the case of a 128×128 Cartesian grid in the transverse dimensions, the root-finding procedure of a shooting-type integration scheme is inappropriate to solve this spatially extended two-point boundary problem, and we are left with a relaxation-type integration scheme.

Equation (B1) cannot be solved exactly, because of the convolution $\widetilde{QA}_2$, which contains the second beam and the grating variable. However, for an infinitesimal propagation distance δz, we assume that the convolution term does not change appreciably, and we are faced with inhomogeneous differential equations, which we formally integrate to yield

$$\tilde{A}_1(z+\delta z)=\tilde{A}_1(z)\exp(ifK^2\delta z) + i\widetilde{QA}_2(z)\frac{\exp(ifK^2\delta z)-1}{fK^2}. \tag{B2}$$

The inverse Fourier transform then determines the field amplitude $A_1(z+\delta z)$ advanced for a δz step. In this manner the first beam is propagated through the nonlinear medium. In an analogous way the second beam, subject to the mirror boundary condition, will be propagated in the backward direction. The grating variable Q does not change during the propagation of the light fields. This is justified by the assumption in our model that the temporal evolution of the grating is much slower than the time needed by the beams to traverse the crystal. However, because of the mirror boundary condition, we are also forced to keep the spatial distribution of one of the beams fixed during the propagation of the other beam. As a consequence, we must iterate the propagation of the beams, alternatingly, until it converges to the solution for a given spatial grating distribution.

Unfortunately, the integration scheme outlined so far fails in converging when strong pump depletion is present, and the relaxation method eventually loses track of the solution during propagation along z. In order to overcome this numerical difficulty, a second-order iteration procedure is necessary. It has the form of an artificial damping added to the field equations,

$$\tilde{A}_1^m(z+\delta z)=\tilde{A}_1^{(\eta=0)}(z+\delta z)-\eta[\tilde{A}_1^m(z)-\tilde{A}_1^{m-1}(z)]. \tag{B3}$$

Here m counts the number of iterations, and $\tilde{A}_1^{(\eta=0)}$ is equal to the rhs of Eq. (B2) at an iteration step m. The artificial damping constant η possesses an optimal value, for which the least iterations are needed. In our simulations $\eta=0.004$.

The relaxation method must, of course, be supplemented with a convergence criterion. We find that the spatial distribution of the light fields is sufficiently approximated, if the transverse-beam profiles at the output faces of the crystal obey the following condition:

$$\int |A_j^m(x,y)-A_j^{m-1}(x,y)|dxdy<\varepsilon\int |A_j^m(x,y)|dxdy. \tag{B4}$$

Accurate results are obtained for $\varepsilon=10^{-6}$. This integral convergence criterion has been checked by a local criterion where necessary. As soon as the beam profiles have converged, the artificial damping term in Eq. (B3) becomes negligible, ensuring that we have found a solution of Eqs. (1).

Once convergence of the beams is achieved, we solve Eq. (2) by advancing the grating amplitude, similar to the field propagation, for an infinitesimal time step δt according to

$$Q(t+\delta t)=Q(t)\exp(-\delta t/\tau) + \frac{\Gamma A_1A_2^*}{|A_1|^2+|A_2|^2+I_d}[1-\exp(-\delta t/\tau)]. \tag{B5}$$

Although one can think of more sophisticated algorithms for the infinitesimal integrations along z and t, they are the least time consuming, and by appropriate choices of δz and δt physically reasonable results are obtained. In our computations both step sizes are always less than 0.05.

[1] M. C. Cross and P. C. Hohenberg, Rev. Mod. Phys. **65**, 851 (1993).

[2] A. C. Newell, Th. Passot, and J. Lega, Annu. Rev. Fluid Mech. **25**, 399 (1993).

[3] C. Bowman and A. C. Newell, Rev. Mod. Phys. **70**, 289 (1998).

[4] H. Haken, *Advanced Synergetics* (Springer-Verlag, Berlin, 1983)

[5] M. Silber and M. R. E. Proctor, Phys. Rev. Lett. **81**, 2450 (1998).

[6] F.-J. Elmer, Phys. Rev. Lett. **70**, 2028 (1993).

[7] F. Matthäus and H. Sauermann, Z. Phys. B: Condens. Matter **99**, 611 (1996).

[8] G. H. Gunaratne, Q. Ouyang, and H. L. Swinney, Phys. Rev. E **50**, 2802 (1994).

[9] B. Pena and C. Perez-Garcia, Europhys. Lett. **51**, 300 (2000).

[10] B. Echebarria and H. Riecke, Physica D **139**, 97 (2000).

[11] J. B. Geddes, R. A. Indik, J. V. Moloney, and W. J. Firth, Phys. Rev. A **50**, 3471 (1994).

[12] D. Engin, M. C. Cross, and A. Yariv, J. Opt. Soc. Am. B **14**, 3349 (1997).

[13] Y. A. Logvin, A. Aumann, M. Tegeler, T. Ackemann, and W. Lange, J. Opt. B: Quantum Semiclassical Opt. **2**, 426 (2000).

[14] P. Lodahl and M. Saffman, Opt. Commun. **184**, 493 (2000).

[15] S. Ciliberto, P. Coullet, J. Lega, E. Pampaloni, and C. Perez-Garcia, Phys. Rev. Lett. **65**, 2370 (1990).

[16] A. C. Skeldon and M. Silber, Physica D **122**, 117 (1998).
[17] B. A. Malomed, A. A. Nepomnyashchii, and M. I. Tribelskii, J. Exp. Theor. Phys. **69**, 388 (1989).
[18] H. W. Müller, Phys. Rev. E **49**, 1273 (1994).
[19] C. Kubstrup, H. Herrero, and C. Perez-Garcia, Phys. Rev. E **54**, 1560 (1996).
[20] W. S. Edwards and S. Fauve, Phys. Rev. E **47**, R788 (1993).
[21] J. P. Gollub and J. S. Langer, Rev. Mod. Phys. **71**, S396 (1999).
[22] R. Herrero, E. G. Westhoff, A. Aumann, T. Ackemann, Y. A. Logvin, and W. Lange, Phys. Rev. Lett. **82**, 4627 (1999).
[23] T. Honda, Opt. Lett. **18**, 598 (1993).
[24] T. Honda, Opt. Lett. **20**, 851 (1995).
[25] P. P. Banerjee, H.-L. Yu, D. A. Gregory, N. Kukhtarev, and H. J. Caulfeld, Opt. Lett. **20**, 10 (1995).
[26] M. Schwab, M. Sedlatschek, B. Thüring, C. Denz, and T. Tschudi, Chaos Solitons Fractals **10**, 701 (1998).
[27] O. Sandfuchs, F. Kaiser, and M. R. Belić, J. Opt. Soc. Am. B **15**, 2070 (1998).
[28] S. G. Odoulov, M. Y. Goulkov, and O. A. Shinkarenko, Phys. Rev. Lett. **83**, 3637 (1999).
[29] C. Denz, M. Schwab, M. Sedlatschek, T. Tschudi, and T. Honda, J. Opt. Soc. Am. B **15**, 2057 (1998).
[30] A. V. Mamaev and M. Saffman, Opt. Lett. **22**, 283 (1997).
[31] M. Schwab, C. Denz, and M. Saffman, Appl. Phys. B: Lasers Opt. **69**, 429 (1999).
[32] M. Schwab, Ph.D. thesis, Darmstadt University of Technology, 2001.
[33] M. Saffman, A. A. Zozulya, and D. Z. Anderson, J. Opt. Soc. Am. B **11**, 1409 (1994).
[34] B. I. Sturman and A. I. Chernykh, J. Opt. Soc. Am. B **14**, 1754 (1997).
[35] T. Honda and P. P. Banerjee, Opt. Lett. **21**, 779 (1996).
[36] P. M. Lushnikov, J. Exp. Theor. Phys. **86**, 614 (1998).
[37] P. Yeh, IEEE J. Quantum Electron. **25**, 484 (1989).
[38] O. Sandfuchs, F. Kaiser, and M. R. Belić, J. Opt. Soc. Am. B **18**, 505 (2001).
[39] R. Martin, A. J. Scroggie, G.-L. Oppo, and W. J. Firth, Phys. Rev. Lett. **77**, 4007 (1996).
[40] A. V. Mamaev and M. Saffman, Phys. Rev. Lett. **80**, 3499 (1998).
[41] J. H. Xiao, G. Hu, J. Z. Yang, and J. H. Gao, Phys. Rev. Lett. **81**, 5552 (1998).
[42] T. Ackemann, B. Giese, B. Schäpers, and W. Lange, J. Opt. B: Quantum Semiclassical Opt. **1**, 70 (1999).
[43] E. Benkler, M. Kreuzer, R. Neubecker, and T. Tschudi, Phys. Rev. Lett. **84**, 879 (2000).
[44] P. Xie, P.-Y. Wang, and J.-H. Dai, J. Opt. Soc. Am. B **17**, 1004 (2000).
[45] E. Ott, C. Grebogi and J. A. Yorke, Phys. Rev. Lett. **64**, 1196 (1990).
[46] K. Pyragas, Phys. Lett. A **170**, 421 (1992).
[47] S. J. Jensen, M. Schwab, and C. Denz, Phys. Rev. Lett. **81**, 1614 (1998).
[48] C. Denz, S. J. Jensen, M. Schwab, and T. Tschudi, J. Opt. B: Quantum Semiclassical Opt. **1**, 114 (1999).
[49] M. Schwab, M. Saffman, C. Denz, and T. Tschudi, Opt. Commun. **170**, 129 (1999).
[50] N. V. Kukhtarev, V. B. Markov, S. G. Odulov, M. S. Soskin, and V. L. Vinetskii, Ferroelectrics **22**, 949 (1979).
[51] N. Singh, S. P. Nadar, and P. P. Banerjee, Opt. Commun. **136**, 487 (1997).
[52] E. Pampaloni, C. Perez-Garcia, L. Albavetti, and S. Ciliberto, J. Fluid Mech. **234**, 393 (1992).
[53] O. Sandfuchs, F. Kaiser, and M. R. Belić, Asian J. Phys. **7**, 629 (1998).
[54] G. P. Agrawal, J. Opt. Soc. Am. B **7**, 1072 (1990).
[55] M. R. Belic, J. Leonardy, D. Timotijevic, and F. Kaiser, J. Opt. Soc. Am. B **12**, 1602 (1995).